Atmos. Chem. Phys., 24, 4511–4535, 2024
https://doi.org/10.5194/acp-24-4511-2024

Atmospheric Chemistry and Physics
Open Access
EGU

The Antarctic stratospheric nitrogen hole: Southern Hemisphere and Antarctic springtime total nitrogen dioxide and total ozone variability as observed by Sentinel-5p TROPOMI

Adrianus de Laat, Jos van Geffen, Piet Stammes, Ronald van der A, Henk Eskes, and J. Pepijn Veefkind

Satellite Observations Department, Royal Netherlands Meteorological Institute (KNMI), De Bilt, the Netherlands

Correspondence: Adrianus de Laat (laatdej@knmi.nl)

Received: 16 October 2023 – Discussion started: 25 October 2023
Revised: 26 January 2024 – Accepted: 15 February 2024 – Published: 17 April 2024

Abstract. Denitrification within the stratospheric vortex is a crucial process for Antarctic ozone hole formation, resulting in an analogous stratospheric "nitrogen hole". Sedimentation of large nitric acid trihydrate polar stratospheric cloud particles within the Antarctic polar stratospheric vortex that form during winter depletes the inner vortex of nitrogen oxides. Here, 2018–2021 daily TROPOspheric Monitoring Instrument (TROPOMI) measurements are used for the first time for a detailed characterization of this nitrogen hole. Nitrogen dioxide total columns exhibit strong spatiotemporal and seasonal variations associated with photochemistry as well as transport and mixing processes. Combined with total ozone column data two main regimes are identified: inner-vortex ozone- and nitrogen-dioxide-depleted air and outer-vortex air enhanced in ozone and nitrogen dioxide. Within the vortex total ozone and total stratospheric nitrogen dioxide are strongly correlated, which is much less evident outside of the vortex. Connecting the two main regimes is a third regime of coherent patterns in the total nitrogen dioxide column–total ozone column phase space – defined here as "mixing lines". These mixing lines exist because of differences in three-dimensional variations of nitrogen dioxide and ozone, thereby providing information about vortex dynamics and cross-vortex edge mixing. On the other hand, interannual variability of nitrogen dioxide–total ozone characteristics is rather small except in 2019 when the vortex was unusually unstable. Overall, the results show that daily stratospheric nitrogen dioxide column satellite measurements provide an innovative means for characterizing polar stratospheric denitrification processes, vortex dynamics, and long-term monitoring of Antarctic ozone hole conditions.

1 Introduction

Stratospheric nitrogen plays a crucial role in catalytic polar stratospheric ozone depletion. That occurs when halogens – mostly chlorine but also some bromine – are massively released from stable reservoir species like $ClONO_2$, HOCl, and HCl (Solomon, 1990; Solomon and Keys, 1992; Dessler, 2000; von Clarmann, 2013). Extremely low stratospheric temperatures during polar winter and the development of the stratospheric polar vortex result in widespread formation of small particles containing nitrogen oxides – forming so-called polar stratospheric clouds (PSCs) – which slowly sediment. This process – called denitrification or denoxification – depletes nitrogen oxides in the polar stratospheric vortex (Farman et al., 1985; Solomon and Garcia, 1983; Salawitch et al., 1989; Fahey et al., 1990; Tabazadeh et al., 2000; Weimer et al., 2023). Strong zonal winds at the stratospheric polar vortex edge prevent resupply of nitrogen oxides from outside the vortex. The return of sunlight to the polar stratosphere during polar spring to the denitrified polar stratosphere leads to the formation of halogen radicals (Solomon, 1999; Santee et al., 2008; Strahan et al., 2014).

The lack of nitrogen oxides – combined with the presence of PSCs – allows the halogen radicals to catalytically destroy ozone. This process causes the rapid formation of the well-known Antarctic ozone hole (Hurwitz et al., 2015). Polar stratospheric ozone depletion ceases when either all ozone is destroyed or the stratosphere becomes warm enough and unfavorable for PSCs while being favorable again for stable halogen reservoir species like HCl (Müller et al., 2008; Strahan et al., 2019; Stone et al., 2021). The warming in turn is caused by increasing sunlight and absorption of that sunlight but sometimes also by increased planetary wave activity (de Laat and van Weele, 2011; Wargan et al., 2020; Smale et al., 2021).

The ozone-depleted Antarctic stratospheric vortex ("ozone hole") is easily identified in, for example, satellite measurements of the total ozone column (TCO_3). It is characterized by a large gradient of ozone-rich outer-vortex air and O_3-depleted inner-vortex air. This gradient is not only present in O_3 but also in other trace gases like nitrogen oxides, as outlined and pioneered by John F. Noxon in the late 1970s (Noxon, 1978, 1979). This cliff-like large vortex-edge trace gas gradient (Schoeberl et a., 1992; Joseph and Legras, 2002; Waugh and Polvani, 2010) is therefore referred to as the "the Noxon cliff". The presence of this cliff reflects air masses on either side of the cliff with very different chemical histories (Dirksen et al., 2011).

Studying Noxon cliff characteristics for a long time depended on numerical modeling (e.g., Solomon and Garcia, 1983; Toon et al., 1989; Garcia and Solomon, 1994; Struthers et al., 2004), ground-based observations (e.g., Gil and Cacho, 1992; Solomon et al., 1993; Kondo et al., 1994; Sanders et al., 1999; Struthers et al., 2004; Bortoli et al., 2005; Yela et al., 2005; Cook and Roscoe, 2009), and aircraft or balloon measurement campaigns over Antarctica (e.g., Goldman et al., 1978; Pommereau and Goutail, 1988; Fahey et al., 1989).

The advance of new innovative satellite instruments from the middle 1990s onwards, but especially after 2000, has enabled exploration of new approaches for monitoring the Antarctic Noxon cliff (Bodeker et al., 2002; Ricaud et al., 2005; Manney et al., 2005; Sato et al., 2009). The use of satellite observations for studying polar stratospheric nitrogen compounds and the Noxon cliff has been predominantly done with satellite limb observations (e.g., Callis et al., 1983; Mount et al., 1984; Rinsland et al., 1996; Haley et al., 2004; Funke et al., 2005; von Savigny et al., 2005; Butz et al., 2006; Davies et al., 2006; Kerzenmacher et al., 2008; Kühl et al., 2008; Kritten et al., 2010; Bourassa et al., 2011; Khosrawi et al., 2011; Sofieva et al., 2012; Belmonte Rivas et al., 2014; Khosrawi et al., 2017; Dubé et al., 2020; Strode et al., 2022; Russell et al., 1984). Note that many of these papers only touch upon the Noxon cliff; i.e., it is seen in the measurements and presented as an example of the observational capacity of a certain satellite and/or data product. Some results have been reported on the use of nitrogen dioxide (NO_2) total columns and/or stratospheric columns for nadir-looking satellites but without a focus on polar regions (Belmonte Rivas et al., 2014; Beirle et al., 2016). Note that a main interest in stratospheric or total NO_2 from nadir-viewing satellites is because of the need to remove the stratospheric component from total column amounts to arrive at the tropospheric NO_2 column (e.g., Hilboll et al., 2013).

There are a few research publications that touch upon satellite nadir total or stratospheric nitrogen dioxide (NO_2) observations over polar regions. Wenig et al. (2004) explore satellite nadir total stratospheric NO_2 (SNO_2) column measurements from the Global Ozone Monitoring Experiment (GOME). They identify the Noxon cliff in Arctic springtime observations in 1997 in relation to the Arctic stratospheric vortex, which persisted much longer than typical during that year. However, they do not explore the Antarctic region for similar purposes even though they mention multiple times that the Noxon cliff is present in both polar regions and that denitrification is larger over Antarctica relative to the Arctic. Richter et al. (2005) also explore GOME observations of total column O_3 (TCO_3), total NO_2 (TNO_2), and OClO over Antarctica during the early 2000s with a focus on the well-known September 2002 Antarctic vortex split (Ricaud et al., 2005; Richter et al., 2005; von Savigny et al., 2005; Yela et al., 2005). They observe strongly reduced inner-vortex SNO_2 during early Antarctic spring that largely vanished after the vortex split. However, no effort has been put into quantitatively correlating TNO_2 / SNO_2 with TCO_3 and/or OClO. Adams et al. (2013) explore some Ozone Monitoring Instrument (OMI) TNO_2 data and TCO_3 data in their study of ground-based observations at the Eureka station in northern Canada in relation to the anomalous longevity of the 2011 Arctic stratospheric vortex. They observe enhanced NO_2 and O_3 when outer-vortex air passes over Eureka associated with photochemical NO_2 production and the stratospheric vortex preventing mixing of outer-vortex air with inner-vortex air, causing NO_2- and O_3-rich stratospheric air to accumulate in the region bordering the Antarctic stratospheric vortex. They also show the conjunction of NO_2- and O_3-depleted inner-vortex air in OMI data. Gordon et al. (2020) explore OMI TNO_2 and TCO_3 in relation to (upper-)stratospheric and mesospheric NO_x formation due to energetic particle precipitation (EEP) but do not explore OMI TNO_2 beyond that application. The Noxon cliff has also been identified in satellite nadir observations of nitrous acid (HNO_3) total columns from the European Infrared Atmospheric Sounding Interferometer (IASI) satellite (Wespes et al., 2009, 2022; Ronsmans et al., 2016) as removal of HNO_3 from the Antarctic stratosphere is the main denitrification process. Those studies showed that – not unexpectedly – Antarctic stratospheric vortex stability was important for inner-vortex HNO_3 and the strength of the Noxon cliff. However, in-depth analysis of the Noxon cliff in IASI HNO_3 observations is also still lacking. Note that strong cross-vortex gradients have also been observed in nadir-viewing satellite measurements of OClO

(Kühl et al., 2006, 2008; Oetjen et al., 2011; Puķīte et al., 2021; Pinardi et al., 2022).

Satellite-observation-based exploration of the Noxon cliff and the denitrification process has thus almost exclusively been restricted to limb-sounding types of satellites. Insofar as can be assessed the use of satellite nadir NO_2 measurements for in-depth study of the Antarctic stratosphere and denitrification has been absent. Even exploitation of the IASI HNO_3 data for this purpose has remained limited – in part also because of the need to average IASI HNO_3 data to reach sufficient data accuracy.

The TROPOspheric Monitoring Instrument (TROPOMI) is the first of the next generation of hyperspectral UV–VIS satellite instruments. Designed and developed based on experience with satellite instruments like GOME, SCIAMACHY (SCanning Imaging Absorption spectroMeter for Atmospheric CHartographY), GOME, and GOME-2 it provides satellite observations of unprecedented spatial resolution and accuracy. Although developed for monitoring tropospheric pollution, total NO_2 column measurements from TROPOMI allow studying stratospheric NO_2 as well since the entire Southern Hemisphere south of approximately 45° S – and thus Antarctica – is devoid of large NO_2 sources. Antarctica is effectively unpopulated and, combined with a moratorium on industrial mining activities, emissions associated with combustion are largely missing. Without much vegetated land, soil NO_x emissions are small and although little is known about the occurrence of lightning near Antarctic the atmospheric conditions do not favor widespread frequent occurrence of lightning. NO_x production due to nitrate photolysis in the Antarctic snowpack is too small to yield tropospheric column amounts measurable by TROPOMI (France et al., 2011; Frey et al., 2013, 2015; Barbero et al., 2021). NO_2 emissions from the largest known single point source in Antarctic – the active volcano Mt. Erebus (Oppenheimer et al., 2005) – are likewise too small to affect NO_x columns on a continental scale. Hence, TNO_2 at high southern latitudes is dominated by SNO_2 columns and the two are thus more or less equivalent. This makes TROPOMI TNO_2 or SNO_2 – in particular combined with its much higher spatial resolution than OMI, GOME-2, and the Ozone Mapping and Profiler Suite (OMPS) – particularly suitable for exploring the Noxon cliff for NO_2 as well as the denitrification–denoxification process.

Furthermore, the current suite of satellites that can be used for stratospheric monitoring is aging and the number of such satellites is dwindling. This is a significant concern for the scientific community and their commitment to monitoring the ozone layer as part of the Montreal Protocol for Protection of the Ozone Layer. Recovery due to the phase-out of emissions of ozone-depleting substances is a slow process and full recovery is only expected in the second half of the 21st century. However, unusual stratospheric events can strongly affect the ozone layer thickness from year to year. Whether such year-to-year changes in stratospheric ozone are anomalous or the result of natural variability is crucial for confident statements on whether recovery is progressing as expected (or not). Satellite instruments measuring the stratospheric chemical composition other than ozone have been essential for understanding this year-to-year variability and thus meeting the commitment of the scientific community to monitoring the ozone layer in support of the Montreal Protocol (WMO, 2022). Given the aging suite of stratospheric monitoring satellites and their dwindling numbers, identifying new stratospheric monitoring applications is more than welcome for continued stratospheric monitoring, especially if these applications are based on satellite instruments that are planned to remain available for many decades into the future.

This paper presents the first steps towards assessing high-spatial-resolution daily TROPOMI TNO_2 and SNO_2 Southern Hemisphere middle- and high-latitude measurements, in particular their relationship with TCO_3. First, the TROPOMI SNO_2 measurements are evaluated by comparison with ground-based Southern Hemisphere and Antarctic SNO_2 column observations. Daily and multi-day TROPOMI TNO_2 measurements are then explored to characterize their spatiotemporal distribution and variability over and around Antarctica during local springtime. Subsequently daily TROPOMI SNO_2 column measurements are collocated with daily TCO_3 data. Similarities and differences in spatiotemporal distributions of both TROPOMI SNO_2 and TCO_3 are identified, analyzed, and discussed. The origins of the complex relation between TCO_3 and SNO_2 in and around the Antarctic stratospheric vortex are briefly hypothesized and recommendations are provided about how satellite data on SNO_2 columns could be further explored and used for studying stratospheric nitrogen.

2 Satellite data sources and data selection

2.1 TROPOMI stratospheric NO_2 data

The Sentinel-5 Precursor (S5P) satellite, launched on 13 October 2017 in an ascending sun-synchronous polar orbit with an Equator crossing at about 13:30 local time, carries the Tropospheric Monitoring Instrument (TROPOMI; Veefkind et al., 2012). This instrument provides measurements from four channels (UV, visible, NIR, and SWIR) of several atmospheric trace gases (such as NO_2, O_3, SO_2, HCHO, CH_4, CO) and of cloud and aerosol properties.

The TROPOMI NO_2 data retrieval is performed from the visible band (400–496 nm), with a spectral resolution and sampling of 0.54 and 0.20 nm, respectively, and a signal-to-noise ratio of around 1500. Individual ground pixels measure in the along-track direction 5.6 km (7.2 km prior to 6 August 2019) and in the across-track direction 3.6 km at the middle of the swath, which increases to about 14 km near the edges of the swath. The full swath is about 2600 km wide, which means that TROPOMI achieves global coverage each day,

except for narrow strips between orbits of about 0.5° width at the Equator.

The NO_2 retrieval process (van Geffen et al., 2020, 2022a, b) uses the three-step approach introduced for OMI (Boersma et al., 2007, 2011). First differential optical absorption spectroscopy (DOAS) is applied to determine the slant column density, the total amount of NO_2 along the effective light path from the sun through the atmosphere to a satellite. A temperature correction is applied to correct for the temperature dependence of the NO_2 cross sections based on collocated temperature profiles from ECMWF (re)analysis data. Then information on the NO_2 vertical profile shape taken from a chemistry transport model–data assimilation system (for TROPOMI: TM5-MP – Transport Model version 5 – Massive Parallel; Williams et al., 2017) that assimilates the slant columns is used to determine the stratospheric vertical column density. The final step determines the tropospheric vertical column using appropriate air mass factors (AMFs). The total vertical column density can be determined either from the sum of the two sub-columns or directly from the retrieved slant column – which of these total columns is the appropriate one depends on the application, as described in the Product User Manual (PUM; Eskes et al., 2021b).

Since nearly all Antarctic NO_2 is located in the stratosphere, this study looks only at SNO_2, the precision of which is estimated to be approximately 2×10^{14} molec. cm^{-2} (3.3 µmol m^{-2}) in the data assimilation. The spatiotemporal variations in SNO_2 are also seen in TNO_2 and the geometric NO_2 column (i.e., the slant column divided by the geometric AMF, i.e., without any model information; see van Geffen et al., 2022a), but not in the tropospheric column. TROPOMI NO_2 data are reported in SI units, i.e., in mol m^{-2}, where the conversion factor to the more commonly used unit molec. cm^{-2} is 6.022×10^{19} mol^{-1}.

The data used for this study come from the version v2.3.1 intermediate S5P-PAL reprocessing over the period 1 May 2018 up to 14 November 2021, followed by the operational v2.3.1 and v2.4.0 processing. The latter version change has little to no impact on the stratospheric NO_2 column and can therefore be ignored in this study. For some information on the different versions, see van Geffen et al. (2022a), the Product Readme File (PRF; Eskes et al., 2021a), and the latest PRF of the operational product (Eskes and Eichmann, 2022).

The stratospheric NO_2 column of all ground pixels with valid retrieval (qa_value > 0.50) of all 14 or 15 orbits of a given day, i.e., orbit files with a start date and time in the file name for that day (irrespective of the actual sensing start and end), is arithmetically averaged on a $0.8° \times 0.4°$ grid (i.e., there are in total 450 by 450 grid cells globally). A qa_value > 0.5 excludes any TROPOMI observation with a solar zenith angle > 81.2. During the Antarctic summer this leads to some observations from the descending TROPOMI orbit over Antarctic being included in the daily average (TROPOMI orbits the sunlit part of the earth from south to north). No weighting in space, in time, or with measurement errors is applied. The daily gridded data are more convenient for various statistical analyses than using daily orbit data, for example for spatiotemporal averaging. We will return in Sect. 4 to the question of whether the gridding and averaging matter for the results presented here.

2.2 TROPOMI stratospheric and/or total NO_2 column validation

It is well established that nadir-viewing satellite measurements of TNO_2 are of good quality (Bortoli et al., 2013). An extensive first global validation of TROPOMI NO_2 can be found in Verhoelst et al. (2021). To highlight the quality of TROPOMI TNO_2 data over and around Antarctica we explore TROPOMI data collocated with ground-based stations from the SAOZ network. The data are conveniently provided and visualized at the TROPOMI validation facility and the on TROPOMI validation server (https://mpc-vdaf.tropomi.eu/index.php/nitrogen-dioxide, last access: December 2022, and https://mpc-vdaf-server.tropomi.eu/no2, last access: December 2022). Extensive evaluation and reports are provided by the validation facility and server as well as in quarterly validation reports (Lambert et al., 2023) where details about the SAOZ data can also be found. We selected five Southern Hemisphere surface stations for comparing SAOZ sunrise data with TROPOMI SNO_2 data from the TROPOMI offline data stream. These five stations are located inside and outside of the vortex and also sample the vortex edge (Table 1). To account for the often large difference in solar local time between the satellite (afternoon) and ground-based (twilight) observations, a diurnal cycle correction is applied based on model calculations. According to Compernolle et al. (2020) and Lambert et al. (2023),

> the SAOZ measurements are adjusted to the TROPOMI overpass time using a model-based factor. This is calculated with the PSCBOX 1D stacked-box photochemical model (Errera and Fonteyn, 2001; Hendrick et al., 2004), initiated with daily fields from the SLIMCAT chemistry transport model (CTM); it is taken here to be 89.5°. The uncertainty related to this adjustment is in the order of 10 %. To reduce mismatch errors due to the significant horizontal smoothing differences between TROPOMI and SAOZ measurements, TROPOMI SNO_2 values (from ground pixels at high resolution) are averaged over the air mass footprint where ground-based zenith-sky measurements are sensitive.

The random error of SAOZ NO_2 total column measurements has been estimated at 4.7 % with a total accuracy of 5.9 % (Hendrick et al., 2011). See Verhoelst et al. (2021) as well as the TROPOMI validation server for more details.

Figure 1a shows a time series of the comparison of TROPOMI stratospheric NO_2 data with the SAOZ observa-

Table 1. Comparison of Southern Hemisphere and Antarctic SAOZ sunrise measurements of SNO_2 (TNO_2) with TROPOMI SNO_2 observations. Correlation coefficients display the Pearson correlation coefficient (P) and the Spearman correlation coefficient (S). Fit coefficients are provided for the ordinary linear regression (OLR; top value) and the orthogonal distance regression (ODR; bottom value).

	R^2 [P] [S]	Bias 10^{15} [mean] [median]	Bias % [mean] [median]	Rms 10^{15} (err)	Rms % (err)	Fit [OLR] [ODR]
Kerguellen (49.35° S/70.26° E)	0.906	−0.038	−2.51	0.291	10.23	0.786
	0.914	−0.065	−2.54	(0.009)	(0.31)	0.818
Rio Gallegos (51.60° S/69.32° W)	0.925	−0.282	−11.39	0.244	9.80	0.899
	0.925	−0.295	−11.62	(0.007)	(0.27)	0.944
Dumont d'Urville (66.67° S/140.02° E)	0.884	−0.039	−0.88	0.371	10.48	0.938
	0.882	−0.056	−1.67	(0.013)	(0.36)	0.999
Neumayer (70.65° S/8.24° W)	0.962	0.091	4.64	0.240	14.01	0.910
	0.960	0.091	4.23	(0.012)	(0.72)	0.926
Concorde Dome (75.1° S/123.35° E)	0.834	−0.035	−2.36	0.466	18.75	0.808
	0.821	−0.130	−3.64	(0.023)	(0.93)	0.875

tions at the Antarctic site of Dumont d'Urville for the period 2018–2022. The Dumont d'Urville site is chosen as it is located sufficiently far north to provide good sampling of the seasonal stratospheric NO_2 cycle while also sampling both inner and outer Antarctic stratospheric-vortex air during local spring. Note that observations are missing during the middle of winter at Dumont d'Urville due to the polar night. Figure 1b shows the scatterplot of the same data.

Overall, the satellite measurements and ground-based measurements at Dumont d'Urville agree well (Table 1). The correlation coefficient is 0.88 (R^2) with a bias of less than 2 % and root mean square differences of approximately 10 %. The regression coefficient equals 0.94 and almost 1.0 dependent on the regression method. The measurements at Dumont d'Urville during Antarctic springtime sample both inner- and outer-vortex air as evidenced by the rapid changes between large and small SNO_2 values during springtime. The validation results for Dumont d'Urville thus cover a wide range of atmospheric conditions. Results for the other four stations are rather similar (Table 1). Figures for the other four chosen validation sites can be found in the Appendix (Figs. A2 and A3) as well as on the TROPOMI validation server. The validation results for all stations can be summarized as follows.

- Correlations (R^2) are always better than 0.80 and up to 0.96.
- Biases are of the order of a few percent (11 % for Rio Gallegos, Patagonia).
- Root mean square differences vary between 10 % and 20 %.
- Standard errors are smaller than 1 %.
- Regression values vary between 0.8 and 0.95.
- Results are fully consistent with Verhoelst et al. (2021).
- Results are fully consistent with Lambert et al. (2023).

Note that for Rio Gallegos the bias is larger than for the other four locations used here (ground-based total NO_2 columns larger than TROPOMI total NO_2 columns). One possible explanation could be that the SAOZ measurement location at Rio Gallegos is within 5 km from the edge of the buildup area of Rio Gallegos and 10 km from the city center. Lambert et al. (2023) found that for 42 polluted locations worldwide Pandora total NO_2 columns were on average approximately 18 % larger than corresponding TROPOMI total NO_2 columns, not unlike the 11 % bias for Rio Gallegos. For low pollution and clean locations the bias was smaller and reversed (TROPOMI total NO_2 columns approximately 6 % larger than Pandora total NO_2 columns). No large dependencies were found for the satellite solar zenith angle (SZA), the satellite cloud fraction, and satellite surface albedo. Given that Rio Gallegos is a city of approximately 80 000 inhabitants and its proximity to the SAOZ measurement site, it is not unlikely that Rio Gallegos SAOZ measurements could be contaminated by local air pollution under favorable wind conditions, although it is beyond the scope of this paper to investigate this in detail. Note that given the large seasonal cycle in total NO_2 columns an 11 % bias is still very acceptable.

Given that the typical seasonal cycle and differences between inner- and outer-vortex air vary by a factor of 2 to 5 and standard errors are a few percent or less combined with very high correlation coefficients and regression coefficients close to 1, single TROPOMI stratospheric NO_2 column measurements are of high quality and likely useful for in-depth exploration of spatiotemporal Antarctic stratospheric NO_2 variability.

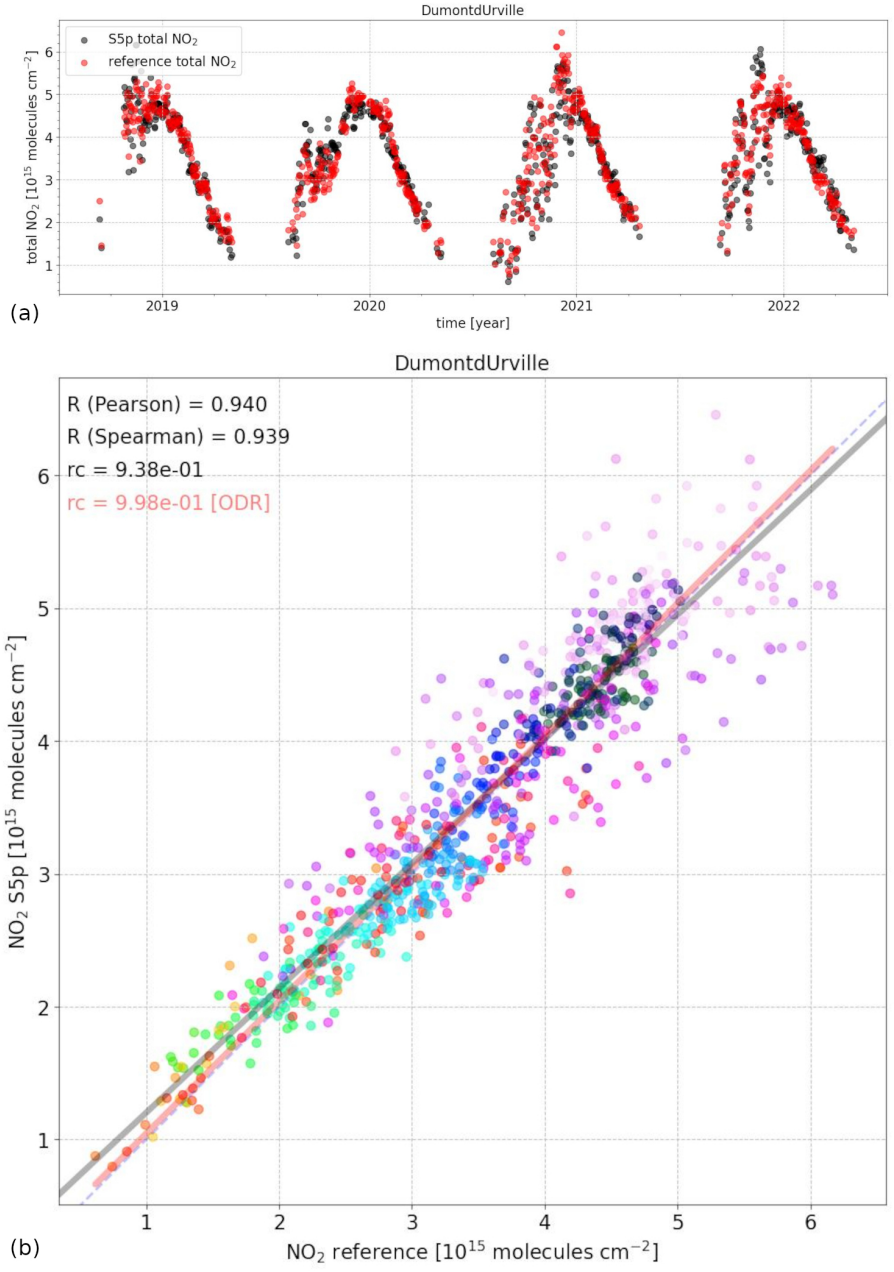

Figure 1. **(a)** Comparison of TROPOMI TNO_2 and SAOZ sunrise TNO_2 for the location of Dumont d'Urville. Data markers are semi-transparent to allow visually discriminating between overlapping SAOZ and TROPOMI data points. Note that for each SAOZ data point there is a corresponding TROPOMI data point. **(b)** Scatterplot of TROPOMI total NO_2 and SAOZ sunrise NO_2 as presented in Fig. 1a. Regression coefficients are for an ordinary linear regression (OLR; grey line) and the orthogonal distance regression (ODR; red line) with 1 : 1 line shown by the grey dashed line. Colors represent different times of the year (see Appendix Fig. A1 for the corresponding colored version of Fig. 1a).

2.3 Global ozone field data

In this study assimilated TROPOMI NO_2 column pixel data are used and gridded at a spatial resolution much coarser than the original TROPOMI resolution while also averaging in time due to multiple polar overpasses per day as the main interest in this first exploratory study is phenomena at continental scales. However, the TROPOMI NO_2 column pixel data are also already post-processed level-2 observations, i.e., TROPOMI NO_2 data derived from a data assimilation system and in that sense not pure level-2 pixel data anymore. Hence, it was decided to compare the TROPOMI NO_2 data with gridded assimilated TCO_3 data rather than

TCO_3 data at orbit level. An obvious TCO_3 dataset to use would be the Multi-Sensor Reanalysis version 2 (MSR-2; van der A et al., 2010, 2015a), which provides a global reanalysis of TCO_3 combining multiple and sometimes overlapping satellite measurements using an advanced ground-data-based approach to minimize inter-satellite-instrument TCO_3 differences and biases. However, the MSR-2 TCO_3 dataset had not yet been extended in time to cover the entire period for which TROPOMI NO_2 data were available. Hence the KNMI operational daily global assimilated TCO_3 field is used here (Eskes et al., 2003; van der A et al., 2015a; https://www.temis.nl/protocols/O3global.php, last access: 6 December 2022), which is based on TCO_3 level-2 data products of the GOME-2 instruments aboard the MetOp satellites (Munro et al., 2006, 2016). This operational TCO_3 field is produced by KNMI for operational UV index predictions up to 9 d ahead in time. GOME-2-based TCO_3 analyses are thus always available in real time – unlike MSR-2, which is currently updated only once per year. From this operational TCO_3 dataset the global total ozone field at each longitude at local solar noon is used, which is close to the TROPOMI measurement time (Sect. 2.1) and which is available for every day of the year for the full globe. The local solar noon ozone field is, for example, used for the operational Tropospheric Emission Monitoring Internet Service (TEMIS) UV index and UV dose processing (van Geffen et al., 2017; Zempila et al., 2017). The local solar noon global TCO_3 field is given at a longitude–latitude grid of $1.5° \times 1.0°$ and is re-gridded (bilinear interpolation) to a finer $0.8° \times 0.4°$ to match the gridded NO_2 data. Note that differences between the KNMI operational daily global assimilated TCO_3 data and the MSR-2 TCO_3 data are small. GOME-2 has a 4 DU offset relative to ground observations (MSR-2 has none), but otherwise GOME-2 and MSR-2 have similar root mean square differences compared to ground observations (van der A et al., 2015a). Hence, for the purpose of this study both datasets would be interchangeable. The question of using assimilated TCO_3 data rather than collocated TROPOMI TCO_3 orbit data will be discussed in Sect. 4.

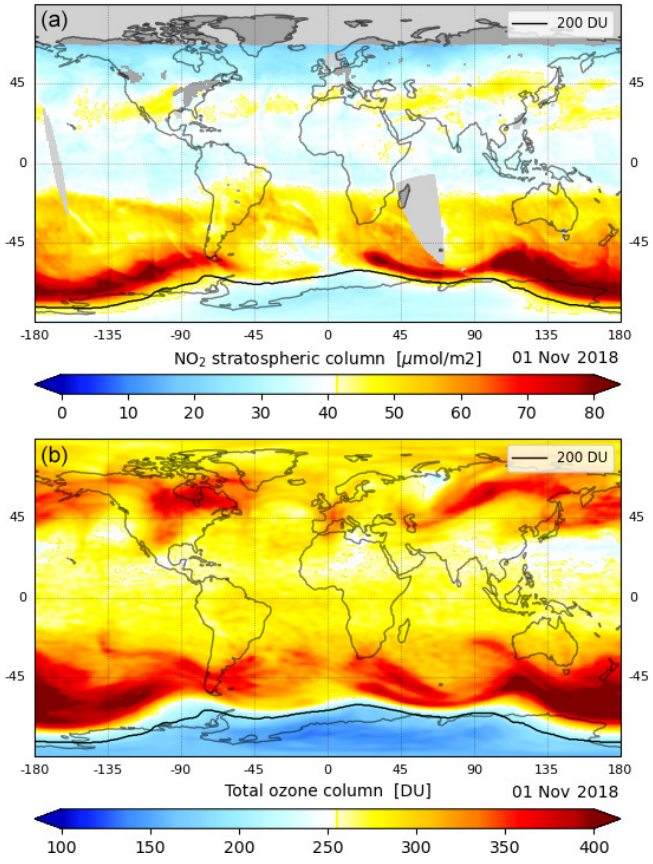

Figure 2. Maps of globally gridded TROPOMI-based stratospheric NO_2 **(a)** (in $\mu mol\,m^{-2}$) and globally gridded local solar noon assimilated TCO_3 **(b)** (in Dobson Units or DU) on 1 November 2018. The location of the 200 DU ozone contour is indicated by a black line in both panels. Grey denotes areas without TROPOMI data.

3 Data analysis and results

3.1 Spatiotemporal variability

Figure 2 shows maps of the spatial distribution of SNO_2 and TCO_3 at local solar noon on 1 November 2018 as an example of daily data. In both panels a black line displays the $TCO_3 = 200$ DU contour, a not uncommon reference value to mark the edge of the Antarctic ozone hole for the Southern Hemisphere polar vortex.

SNO_2-depleted Antarctic inner-vortex air and enhancement of SNO_2 around the edge of the polar vortex are clearly visible. Figure 3 shows the same data as in Fig. 2 but for an Antarctic polar view and with a different color scale. There are clear similarities between the spatial patterns in SNO_2 and TCO_3. First of all, both show a significant reduction of values within the Antarctic stratospheric vortex. Secondly, values for both are strongly enhanced equatorward just outside of the vortex. Third, further equatorward of 45° S values of both start to decrease. And fourth, outside of the vortex values for both are reduced around 0° longitude and enhanced at the opposite side towards 180° longitude (wave-1 pattern).

However, there are also clear differences. The SNO_2 / TCO_3 ratio, for example, does not show a clear vortex edge (Noxon cliff) like in both separate products. Furthermore, the gradient from the vortex edge towards the Equator is smaller for TCO_3 than it is for SNO_2. These similarities and differences point to different processes governing their respective spatiotemporal variations: chemistry (sources and sinks) and stratospheric dynamics (source and sink regions and transport from sources to sinks).

Figure 4 shows the evolution of zonal averages of SNO_2 during the four Southern Hemisphere summers from 2018 to 2021, with the 200 DU ozone contour indicated by a black

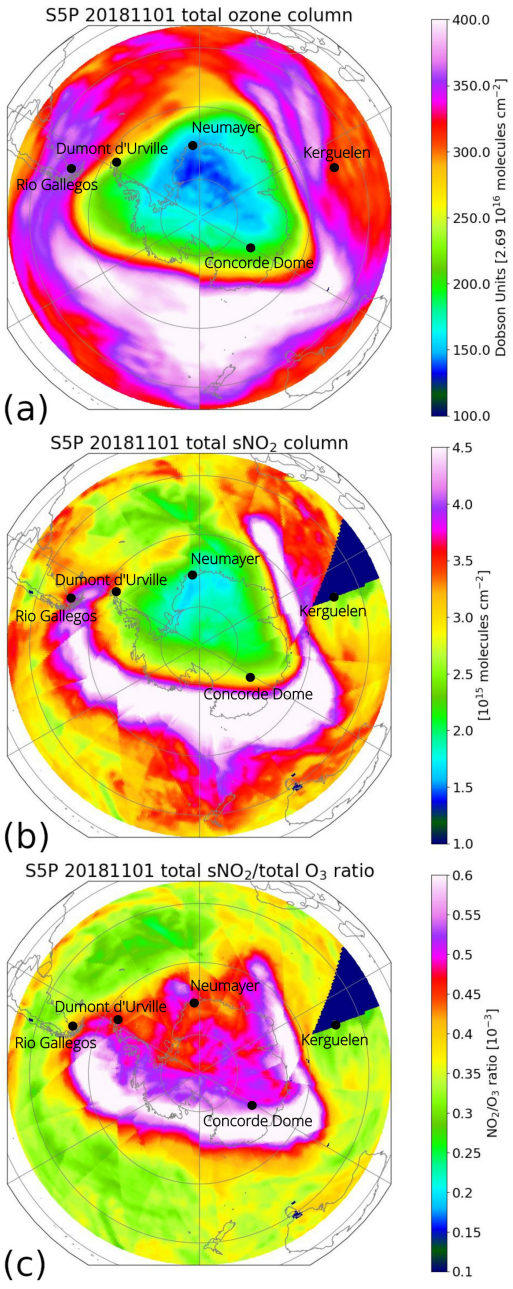

Figure 3. As Fig. 2 (1 November 2018) but from an Antarctic polar view and with a different color scale. Panel **(c)** shows the SNO_2 / TCO_3 ratio of panels **(a)** and **(b)**.

line. From these figures it is clear that springtime advection of SNO_2-enhanced stratospheric air into the Antarctic stratospheric vortex is limited during 2018, 2020, and 2021. The lack of such a well-defined SNO_2-depleted area in 2019 is related to the weak Antarctic stratospheric vortex during spring 2019, which led to weak ozone depletion (Safiedinne et al., 2020; Wargan et al., 2020; Stone et al., 2021) and according to the TROPOMI NO_2 data thus also led to less denitrification. This is consistent with results from IASI HNO_3 (Wespes et al., 2022).

3.2 Correlating SNO_2 and TCO_3: 2D phase diagram

Figure 5 displays TROPOMI TCO_3 and SNO_2 data for 1 November 2018 as a 2D histogram (phase diagram; Fig. 5a) revealing rather intricate patterns. For reasons explained below, the histogram was divided into three areas to be able to discriminate between the inner vortex (MASK-1), outer vortex (MASK-2), and vortex edge (MASK-3). For the area MASK-1 SNO_2 and TCO_3 show a well-defined linear relationship. The area is associated with the inner vortex and is characterized by small TCO_3 values. The area MASK-2 represents air outside of the vortex characterized by larger TCO_3 values and somewhat larger SNO_2 values than for the MASK-1 area. Also, there is not such a well-defined linear relation between TCO_3 and SNO_2 for the MASK-2 area as there is for the MASK-1 area. The relation between TCO_3 and SNO_2 for MASK-3 is much more intricate with what appear to be "coherent line structures" connecting the MASK-1 and MASK-2 areas. These "mixing lines" – for lack of a better expression – are found for both small and large TCO_3 and SNO_2 values. The largest SNO_2 values are found in the MASK-1 and MASK-3 areas, whereas the largest TCO_3 values are found in the MASK-2 and MASK-3 areas. Note that the logarithmic color scale enhances the focus on parts of the distribution that are less frequent. There are thus essentially two populations: inside the vortex and outside the vortex. A total of 16 % of the histogram bins contain two-thirds (∼ 67 %) of the data points and only approximately 10 % of the data qualify for MASK-3.

3.3 Multi-day periods and multi-annual data

A key follow-up question is whether these results change significantly over time. Figure 6 shows phase diagrams similar to the one displayed in Fig. 5 but for days combined during multiple-day intervals (5, 10, 15, and 30 d) starting at 1 November 2018. Although this means that each panel covers a different time period, the results are nevertheless very consistent. The distinction of two clear concentrated populations and the mixing lines is present for each time period. The results also reveal a relation between TCO_3 and SNO_2 outside of the vortex, albeit with a much larger spread. The high correlation between TCO_3 and SNO_2 inside the vortex is also present during all periods. The distribution does shift towards larger SNO_2 values due to increasing SNO_2 as part of the natural springtime SNO_2 cycle. Similarly, although more difficult to distinguish in Fig. 6, outer-vortex TCO_3 values become slightly smaller due to the natural seasonal springtime non-catalytic photochemical destruction of stratospheric O_3. However, for inner-vortex air the TCO_3 distribution shifts towards larger TCO_3 values, reflecting the effects of dynamical

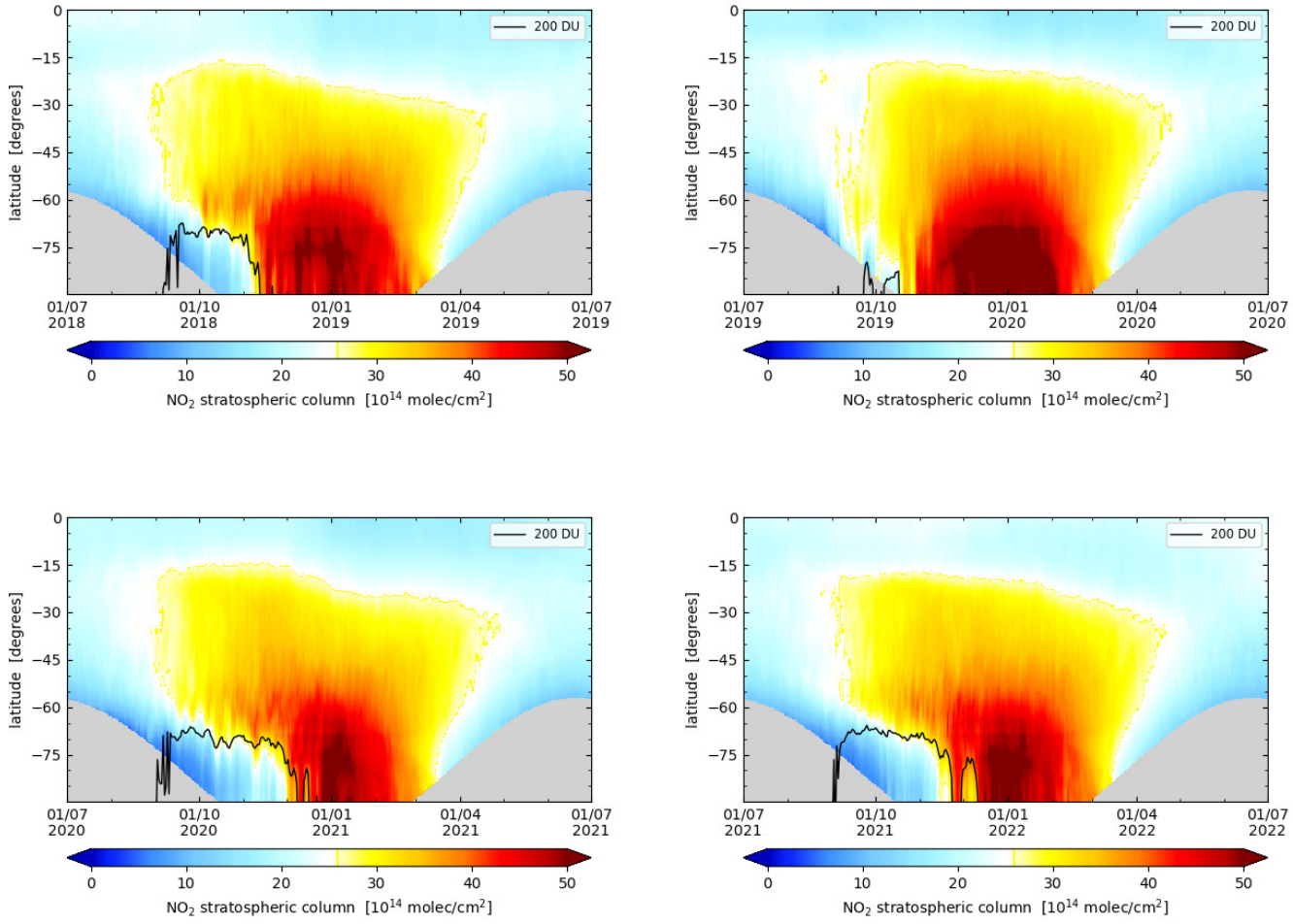

Figure 4. Maps of the Southern Hemisphere daily zonal average SNO_2 for four Southern Hemisphere summers (July–July) from 2018 to 2022. The location of the 200 DU ozone contour is indicated by a black line in all panels. Grey denotes areas and times within TROPOMI data.

mixing of extra-vortex O_3-rich (upper-)stratospheric air during late spring (de Laat and van Weele, 2011).

Figure 7 shows similar panels as in Figs. 5 and 6 but for 5 d periods starting at the first day of each month from September to December 2018. The results are much more variable than for the multi-day differences, highlighting the strong seasonality of Antarctic stratospheric inner-vortex TCO_3 and SNO_2. During early September O_3 depletion has yet to commence. There are already two separate populations discernible but TCO_3 values are still larger than 200 DU. SNO_2 values are generally small, especially within the Antarctic vortex due to the denitrification process. In early October 2018 the catalytic O_3 destruction has strongly reduced stratospheric O_3. There is a group of data points with small TCO_3 values and small SNO_2 values. The air outside of the vortex is still characterized by large TCO_3 values and still relatively small SNO_2 values but larger values than during early September 2018. The mixing lines are also clearly discernible, covering the entire phase space between the two main populations. The picture for early November 2018 is rather similar, although SNO_2 values have further increased due to the natural seasonal cycle in SNO_2. By early December 2018 the distribution is squeezed and values from both main populations are closer together. The vortex has largely disintegrated, although remnants can still be discerned in TCO_3 but interestingly enough not in SNO_2 (see animation in the Supplement). Remarkably the populations still cover the three previously defined areas MASK-1, MASK-2, and MASK-3. This indicates that TCO_3 / SNO_2 ratios are rather useful for characterizing the origins and locations of stratospheric air masses.

Figure 8 displays similar results as in Fig. 7 for early October but for all years from 2018 to 2021. The results for 2018, 2020, and 2021 are very similar, providing further support for the notion that the TCO_3 / SNO_2 ratios can be used to characterize the origins and locations of stratospheric air masses. The results for 2019 are quite different, reflecting the unusually weak 2019 Antarctic stratospheric vortex. There are still

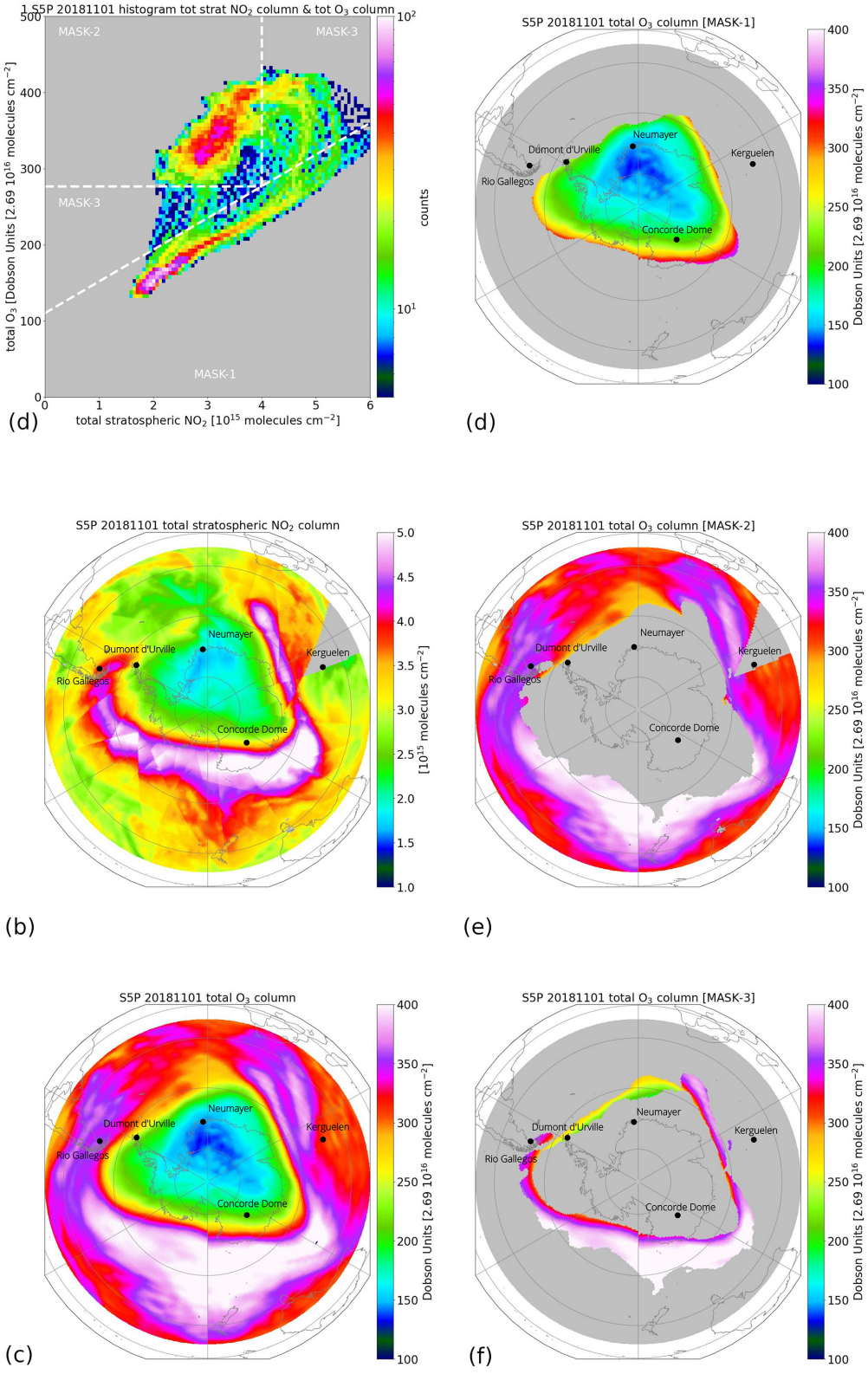

Figure 5. **(a)** 2D histogram (phase diagram) of TROPOMI SNO_2 vs. assimilated TCO_3 for 1 November 2018 and corresponding spatial distribution of SNO_2 **(b)** and TCO_3 **(c)** as in Fig. 3. The phase diagram is color-coded according to the logarithm of the number of counts. The phase diagram is a 100×100 pixel grid ranging between 0.0–6.0 $\times$ 10^{15} molec. cm^{-2} SNO_2 and 0–500 DU TCO_3. **(d–f)** Spatial distribution of TCO_3 as in the lowest plot of the left column but filtered on the masking in the phase diagram in the upper left plot. **(d)** MASK-1, **(e)** MASK-2, **(f)** MASK-3.

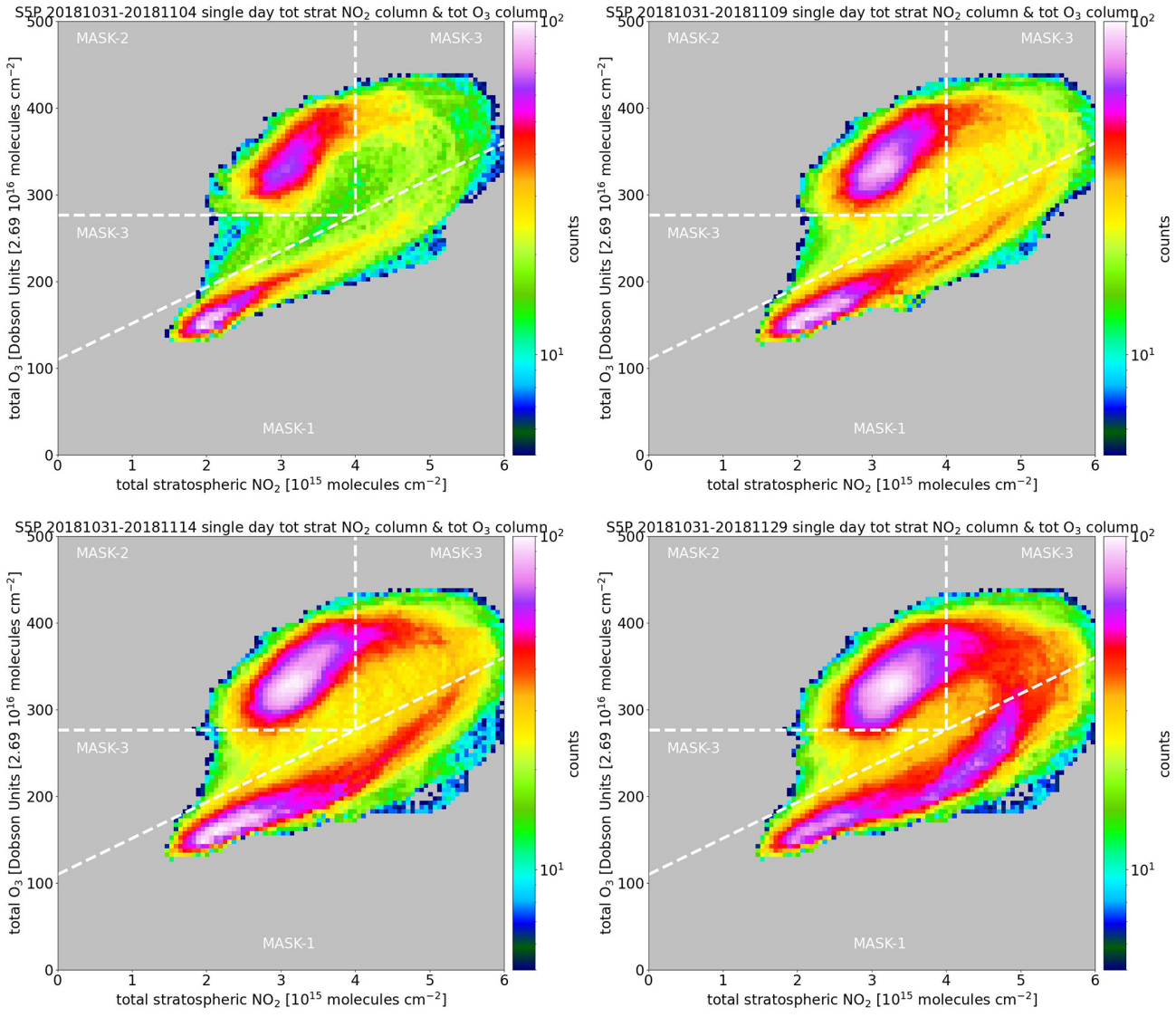

Figure 6. Phase diagrams of TROPOMI SNO_2 and assimilated GOME-2 TCO_3. Similar to the phase diagram in Fig. 5a but for daily gridded data combining either 5, 10, 15, or 30 d starting at 31 October 2018.

two populations in 2019 but only weakly separated. TCO_3 and SNO_2 values inside the vortex are larger compared to the other years. Overall, the anomalous 2019 vortex has a clear imprint on the TCO_3 and SNO_2 distributions. Note that during early September 2019 the amount of SNO_2 depletion was still similar to those in 2018, 2020, and 2021 (not shown). The normal vortex pre-conditioning during austral winter 2019 was thus not unusual, which is consistent with published analyses of the 2019 Antarctic springtime vortex (Wargan et al., 2020; Smale et al., 2021; WMO, 2022). The faster 2019 increase in SNO_2 by early October compared to 2018, 2020, and 2021 indicates that dynamics and mixing with – or influx of – NO_2-rich extra-vortex air are the main cause. Otherwise the SNO_2 increase would have been slower and more in line with the other 3 years.

3.4 Qualitative explanation of phase diagram results

The consistency of patterns in the spatiotemporal variations in the TCO_3–SNO_2 distributions suggests some very basic underlying processes. For example, differences in the location of the TCO_3 cross-vortex gradient relative to the location of the Noxon cliff for SNO_2 should show up as patterns in the phase diagram. To provide a qualitative explanation of the observed patterns two simple series of longitudinal and latitudinal variations in TCO_3 and SNO_2 were created. For the first one, TCO_3 and SNO_2 vary as a sine wave along longitudes but with a different longitudinal phase (Fig. 9). For the second one, TCO_3 and SNO_2 increased from the poles to middle latitudes and then decreased toward the Equator to resemble the Noxon cliff but with a slightly different lat-

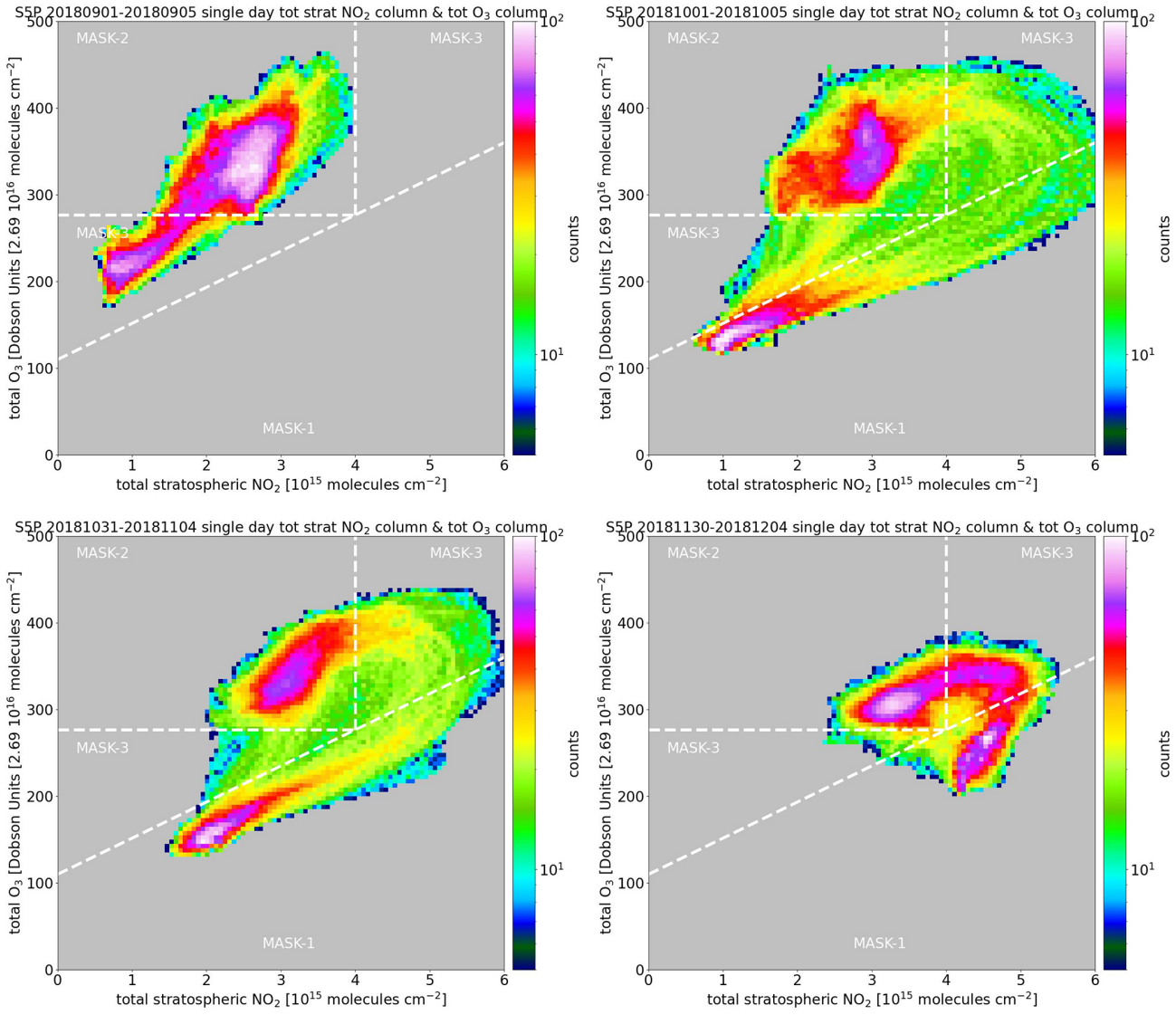

Figure 7. As Fig. 6 but for 5 d periods starting at 1 September, 1 October, 31 October, and 30 November 2018.

itudinal change visually mimicking the observed TCO_3 and SNO_2 latitudinal gradients. Figure 9 shows the results for the relation between the two. For the phase-shifted sine wave functions, the results obviously show up as an oval. The latitudinal shifted results, however, follow a curve not qualitatively dissimilar from the observed mixing lines. These results thus support the observation that the cross-vortex TCO_3 gradient and SNO_2 Noxon cliffs do not occur at the same locations, which results in the emergence of mixing lines in the phase diagrams.

4 Discussion

The results presented here show that TROPOMI provides high-quality daily SNO_2 data for monitoring variations in SNO_2 both inside and outside the Antarctic stratospheric vortex. It allows for studying the nitrogen hole, the denitrification process, and the Noxon cliff – the sharp gradient in trace gas amounts along the vortex edge – as well as associated seasonal changes during Antarctic springtime and interannual variability. Furthermore, combining the SNO_2 data with high-quality TCO_3 data in phase diagrams reveals coherent patterns – mixing lines – linking the Antarctic stratospheric air inside and outside the vortex.

A clear discrepancy was found between the location of the SNO_2 Noxon cliff and the TCO_3 cross-vortex gradient. The few studies that provide information on the joint vertical distributions of NO_2 and O_3 suggest that the bulk of stratospheric NO_2 is found at higher altitudes than the bulk of stratospheric O_3 (Ridley et al., 1984; Lindenmaier et al., 2011). Differences in bulk heights, which mostly determine total column variability, link to differences in advec-

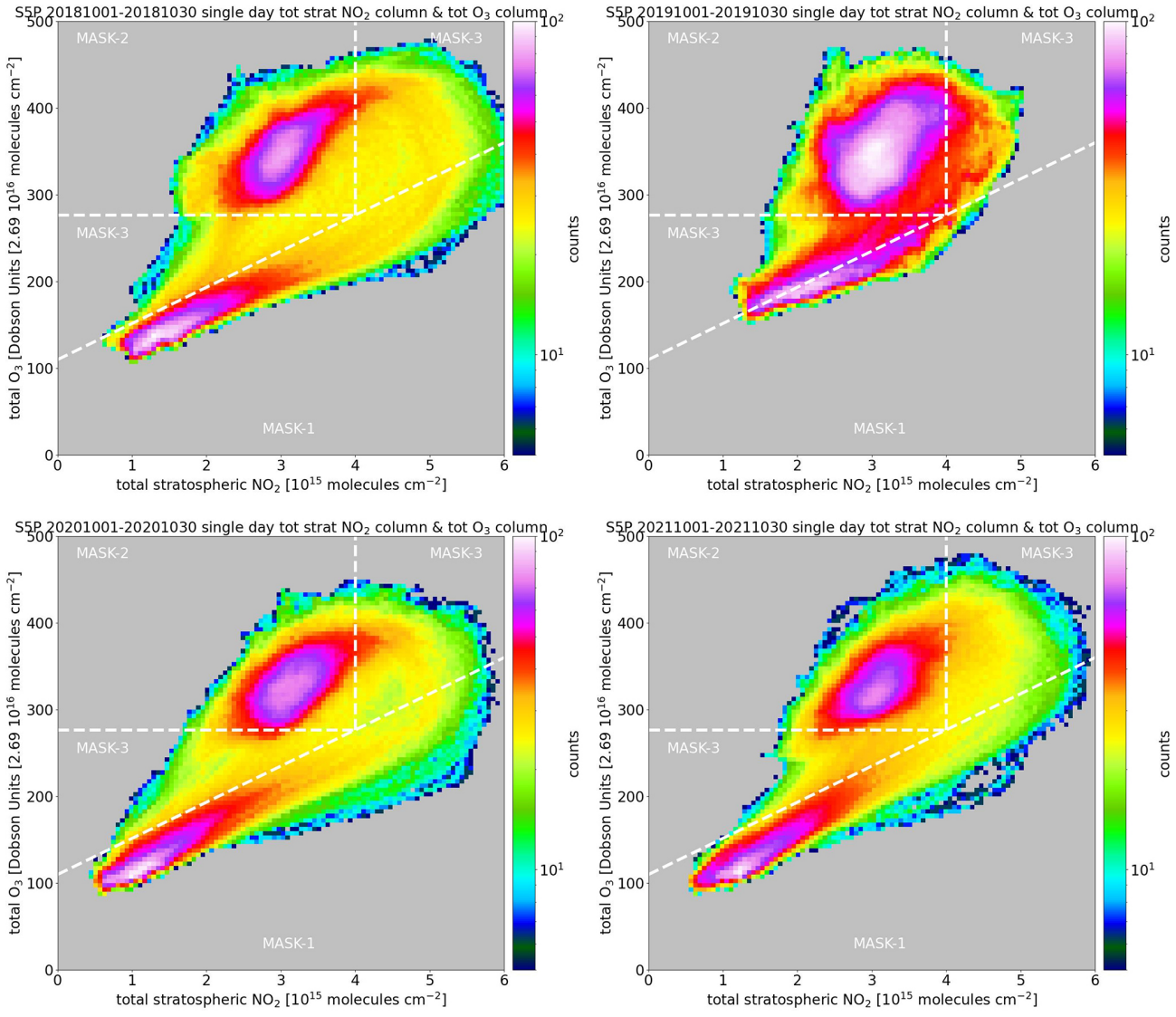

Figure 8. As Fig. 6 but for 1–30 October of each year between 2018 and 2021.

tion processes and might explain differences in the location of the NO_2 Noxon cliff and the cross-vortex TCO_3 gradient. Explorative studies using stratospheric chemistry models should likely help unravel these issues. This in turn may contribute to developing applications and metrics for stratospheric NO_2-column-based Antarctic ozone hole monitoring. In addition, the notion of different bulk heights is consistent with the notion that the break-up dates or final warming of the Antarctic stratospheric vortex occurs later for lower-stratospheric altitudes (higher pressure levels) (Butler and Domeisen, 2021; Lecouffe et al., 2022). For example, by late November 2018 there is still a well-defined area with reduced TCO_3 for which reduced SNO_2 has already vanished (see animation in the Supplement). A lower bulk height for TCO_3 compared to SNO_2 would mean that SNO_2 anomalies would vanish earlier, as observed.

Furthermore, a strong inner-vortex correlation between SNO_2 and TCO_3 was found, which was absent outside of the vortex. The SNO_2–TCO_3 phase diagrams display a clear dynamical cycle reflecting springtime changes in chemistry and dynamics. This cycle was consistently seen in multiple years (2018, 2020, and 2021) but was significantly different in 2019, a year with a strongly perturbed Antarctic springtime vortex. Qualitatively the coherent patterns in the phase diagrams can be explained by spatiotemporal differences in the phases of SNO_2 and TCO_3, i.e., where and when minima and maxima occur in SNO_2 and TCO_3. SNO_2 and TCO_3 are clearly not always in sync everywhere. This in part appears to be associated with the differences in Antarctic stratospheric denitrification and O_3 depletion. Denitrification is a wintertime process already starting by early winter and causing the Antarctic stratosphere to be significantly depleted of nitro-

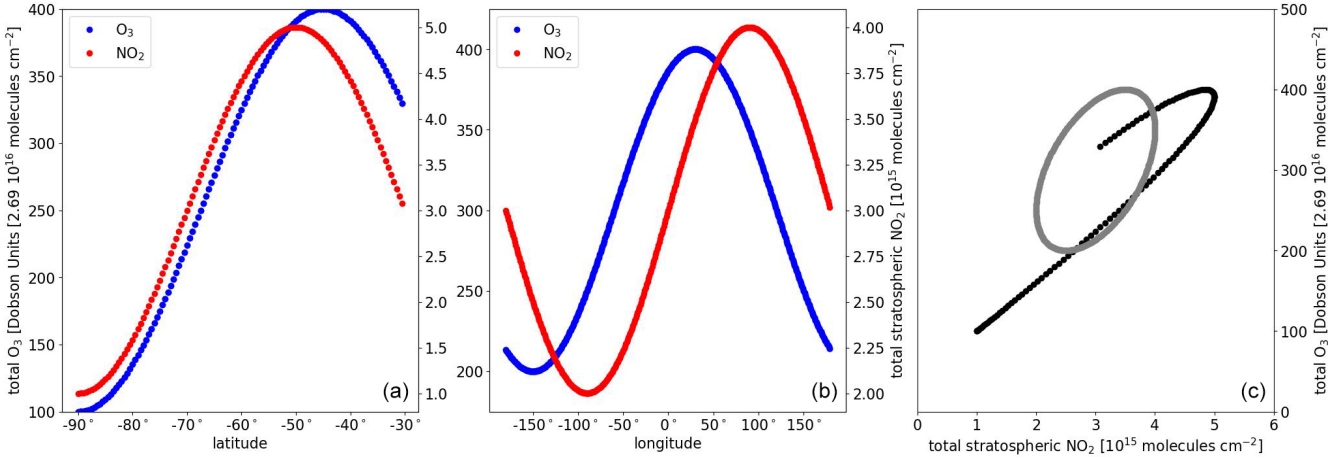

Figure 9. **(a)** Latitudinal SNO_2 and TCO_3 variations between 30 and 90° S. The functions for SNO_2 and TCO_3 are slightly shifted in the latitudinal direction, with SNO_2 peaking earlier and decreasing faster towards the Equator after the peak. The result of these two functions is indicated by the black line in panel **(c)**. **(c)** Longitudinal data and phase diagram of a data series (sine wave) for SNO_2 (red) and TCO_3 (blue) with a longitudinal phase shift of 90°. The amplitude of the sine wave is chosen to represent observed values but otherwise just a scaling factor. The result for these two functions is indicated by the grey line in panel **(c)**.

gen by the time sunlight returns (and thus TROPOMI starts to provide inner-vortex observations). The O_3 destruction cycle, on the other hand, critically depends on the presence of sunlight. At the start of springtime O_3 depletion has yet to speed up. During the month of September the amount of sunshine and duration of sunshine rapidly increase, causing a rapid deepening of the Antarctic ozone hole. Hence, the denitrification and O_3 depletion cycles differ significantly in their timing. Similarly, the results also revealed an earlier disappearance of the NO_2 hole relative to the ozone hole, further supporting the notion that differences in chemistry and dynamics govern the differences in SNO_2 and TCO_3 behavior.

The observation of coherent spatial line structures (mixing lines) in relation to stratospheric transport and mixing – including stratosphere–troposphere exchange – is not new. The presence of layered trace gas structures in the stratosphere (laminae, filamentation, contour advection; Waugh and Plumb, 1994; Newman et al., 1996; Appenzeller and Holton, 1997; Orsolini and Grant, 2000; Koh and Legras, 2002) is closely associated with the stability of the stratosphere, the conservation of potential vorticity, and isentropic mixing (Waugh and Polvani, 2010). Stratospheric air masses often organize themselves in such long-lived laminae. For example, satellite observations of direct injection of volcanic material directly into the (lower) stratosphere have provided many examples of laminae development and filamentation because of the ability of satellites to observe sulfur dioxide and volcanic ash (Krotkov et al., 2021; de Leeuw et al., 2021; Khaykin et al., 2022). Satellite observations of aerosols from wildfires have started to be used for similar purposes for stratospheric smoke (Khaykin et al., 2020; Magaritz-Ronen and Raveh-Rubin, 2021). And complex relationships among (long-lived) stratospheric trace gases have been used for understanding stratospheric dynamics (e.g., Hoor et al., 2002; Plumb, 2007; Barré et al., 2012; Hoffmann et al., 2017; Krasauskas et al., 2021). How exactly these processes and concepts relate to the observed mixing lines would make a relevant topic of future research.

Furthermore, model simulations could be used to assess (1) whether model simulations show similar phase diagrams and, if so, (2) whether the model simulations contain clues for explaining the differences in spatiotemporal SNO_2 and TCO_3 behavior. The model simulations might also reveal caveats and missing processes in the model representation of stratospheric chemistry and Antarctic stratospheric vortex dynamics. In addition, the results can also be further explored towards a more thorough conceptual explanation of SNO_2 variability. Comparison with IASI HNO_3 total columns might help there as well, just like a comparison and evaluation of SNO_2 with satellite NO_2 profile measurements from, for example, the OSIRIS (Optical, Spectroscopic and Infrared Remote Imaging System), ACE-FTS (Atmospheric Chemistry Experiment – Fourier Transform Spectrometer), or MAESTRO (Measurements of Aerosol Extinction in the Stratosphere and Troposphere Retrieved by Occultation) satellite instruments. A comparison with IASI HNO_3 could, for example, be used to explore whether both are more in sync than SNO_2 is with TCO_3. Comparison with limb satellite NO_2 profile measurements in conjunction with O_3 profile measurements should provide indications of which altitudes mostly determine column observations of NO_2 and O_3. In addition, evaluation of results from a different dynamical framework of the equivalent latitude might help improve understanding of Antarctic stratospheric vortex-edge dynamics. This links to the important question of where and when vortex mixing takes place. It is well es-

tablished that the Antarctic stratospheric vortex can be destabilized by increased extra-vortex wave activity. Direct observations of where and when that takes place are unclear but the combination of SNO_2 and TCO_3 (possibly extended with IASI HNO_3) might help identify mixing regions.

An additional question is whether satellites other than TROPOMI that also measure SNO_2 might help extend the SNO_2 Southern Hemisphere record further back in time. A dataset going back to 2003 already exists via the QA4ACV NO_2 data (Quality Assurance for Essential Climate Variables; Boersma et al., 2018). The combination of GOME (1995–2011), SCIAMACHY (2002–2012), OMI (2003–now), GOME-2 (2007–now), and OMPS (2012–now; Ozone Mapping and Profiler Suite) potentially allows for reconstructing an almost 30-year record of Southern Hemisphere midlatitude and Antarctic SNO_2. Such a record could be probed for finding hints and clues of (Antarctic) stratospheric ozone recovery, as TCO_3 is expected to change much faster due to decreasing O_3-depleting substances than SNO_2 – mostly due to emissions of N_2O and slowly increasing atmospheric N_2O concentrations (Struthers et al., 2004). Other processes relevant for Antarctic stratospheric NO_2 and O_3 are production of (upper-)stratospheric NO_x by energetic electron precipitation and by increased downwelling of upper-stratospheric air by the expected speeding up of the Brewer–Dobson circulation (Gordon et al., 2020; Maliniemi et al., 2021; Müller, 2021).

Furthermore, there are some other aspects for further exploration. The validation could be extended to more ground-based comparison and more detailed evaluations. It could be assessed whether it matters if TNO_2 is used (based on data assimilation) rather than SNO_2. The assimilation SNO_2 data are important for deriving tropospheric NO_2 but not necessarily the best estimate of TNO_2. Note that there is no reason to assume that SNO_2 and/or TCO_3 data quality issues will change the findings of this paper, but only in-depth analyses will provide support for that assumption. In addition, although the diurnal cycle in SNO_2 is relatively small compared to its seasonal cycle it nevertheless can affect satellite retrievals and validation results. Dubé et al. (2021) reported order-of-magnitude 10 %–20 % diurnal cycle effects for SAGE III/ISS solar occultation limb retrievals with the largest effects found at higher latitudes. Although their results are not one-on-one applicable to the results presented here they clearly indicate the need for properly assessing diurnal cycle effects on TROPOMI SNO_2 measurements and validation.

In this study gridded SNO_2 was used to allow easy comparison with other data as TROPOMI data quality is still improving and reprocessing of data is ongoing. A key question is whether results would differ for a TROPOMI pixel-level comparison of SNO_2 and TCO_3. A first brief assessment of using TROPOMI pixel-level comparison of SNO_2 and TCO_3 (see Appendix Fig. A4) yielded very similar results, indicating that results presented here are robust relative to using gridded data, pixel data, or even data from different satellites.

Finally, limited use of nadir-viewing satellite measurements of NO_2 for studying the Noxon cliff and the Antarctic stratospheric denitrification process is somewhat surprising. The potential for their use to explore polar stratospheric chemistry and dynamics is evident from Wenig et al. (2004), Richter et al. (2005), and Adams et al. (2013). Satellite measurements of NO_2 – and tropospheric NO_2 column measurements – have been widely used for approximately 2 decades now. Total stratospheric NO_2 columns play an important role in deriving tropospheric NO_2 columns, as the stratospheric part needs to be removed from the total part (Boersma et al., 2004, 2007, 2018). This is typically done by assimilating the satellite measurements of total NO_2 over clean regions into a numerical chemistry transport model to reconstruct the stratospheric column globally (Eskes et al., 2003; Boersma et al., 2004, 2007). The assimilation therefore allows determining the stratospheric column over polluted regions with sufficient accuracy and precision to subtract it from the total column to arrive at an accurate tropospheric column. This approach also requires sufficiently accurate measurements of stratospheric NO_2. Hence the quality of stratospheric NO_2 has for a long time been assessed for various satellites (e.g., Boersma et al., 2004; Dirksen et al., 2011; Valks et al., 2011; Verhoelst et al., 2021; Lambert et al., 2023). Nevertheless, despite the fact that nadir stratospheric NO_2 column TROPOMI measurements turn out to be of very good quality their intrinsic value for stratospheric research has remained largely unrecognized.

5 Conclusions

This paper presents a first assessment of the use of Sentinel-5p TROPOMI SNO_2 measurements for studying Southern Hemisphere middle-latitude and Antarctic stratospheric processes including the Antarctic ozone hole.

Comparison of gridded SNO_2 and assimilated TCO_3 via phase diagrams reveals intricate patterns. Three different regimes could be clearly identified: the inner vortex, the vortex edge, and the extra-vortex region. Each regime is associated with its own SNO_2 / TCO_3 characteristics. The vortex edge was characterized by so-called "mixing lines" in SNO_2–TCO_3 phase diagrams. A certain misalignment of the SNO_2 Noxon cliff and cross-vortex TCO_3 gradient was found along the Antarctic stratospheric vortex, pointing to vortex-edge dynamics as the root case. A possible explanation could be differences in bulk heights of SNO_2 and TCO_3 so that their respective total columns reflect processes occurring at different heights.

Springtime SNO_2–TCO_3 variations and changes are robust throughout single-day to multi-day statistics. Throughout spring the SNO_2–TCO_3 distributions change significantly as a result of chemistry and vortex dynamics including

mixing of air inside and outside the vortex. Regarding interannual variability the distributions are very similar for 2018, 2020, and 2021 but significantly different from 2019, which was a year with an anomalously weak Antarctic stratospheric vortex and only weak O_3 depletion.

Seasonal changes in the phase diagrams indicate that both total column data products are sensitive to different heights and thus different processes. In general the vortex remains visible longer in TCO_3 data than in SNO_2 data. SNO_2 is less sensitive to the lower stratosphere – where the stratospheric vortex remains intact longer – than SNO_2 so the nitrogen hole will disappear earlier than the ozone hole. Vertical tilting of the vortex edge combined with different vertical sensitivities likewise explains the presence of the third regime: that in the phase diagrams linking the inner-vortex regime with the outer-vortex regime.

This study only presents a first glimpse of the great potential of high-quality spatiotemporal satellite SNO_2 measurements for studying stratospheric chemistry and stratospheric dynamics as well as long-term changes in stratospheric composition extending the SNO_2 record back in time in combination with, for example, the MSR-2 total ozone reanalysis (van der A et al., 2015a). The ability to monitor stratospheric nitrogen is also more than welcome given that an important piece of stratospheric observational remote sensing capacity by way of the Microwave Limb Sounder (MLS) will end by 2025 or at the latest 2026 and no satellite missions are planned to fill the gap created by the end of the MLS mission.

Appendix A

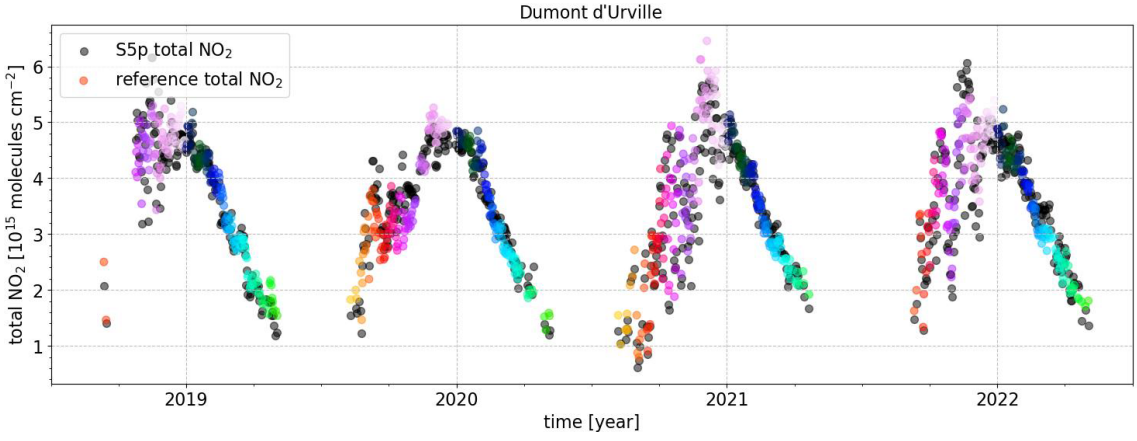

Figure A1. As Fig. 1a but color-coded according to time of the year (color coding also used in Fig. 1b).

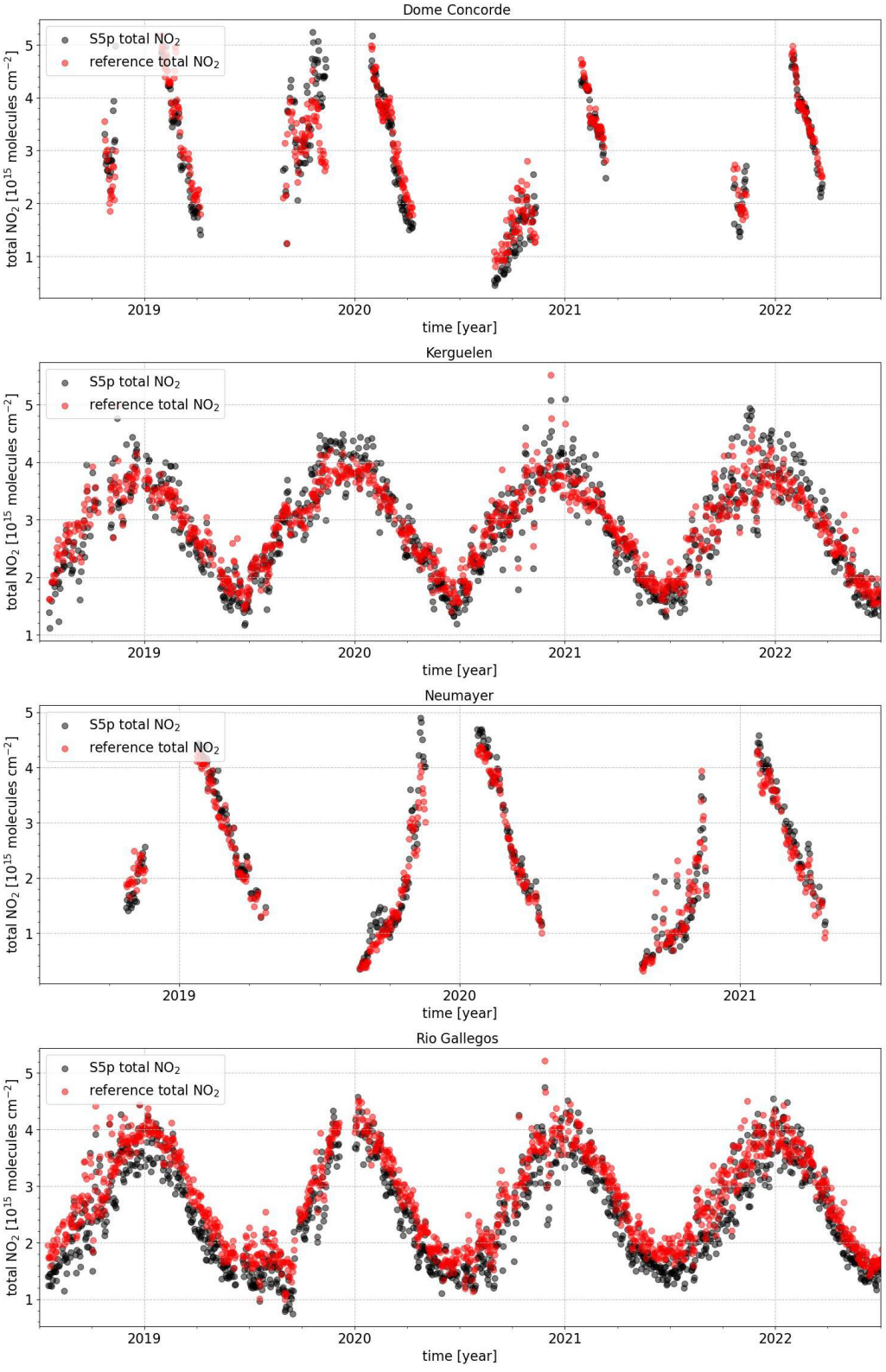

Figure A2. As Fig. 1a but for the other surface measurement stations in Table 1.

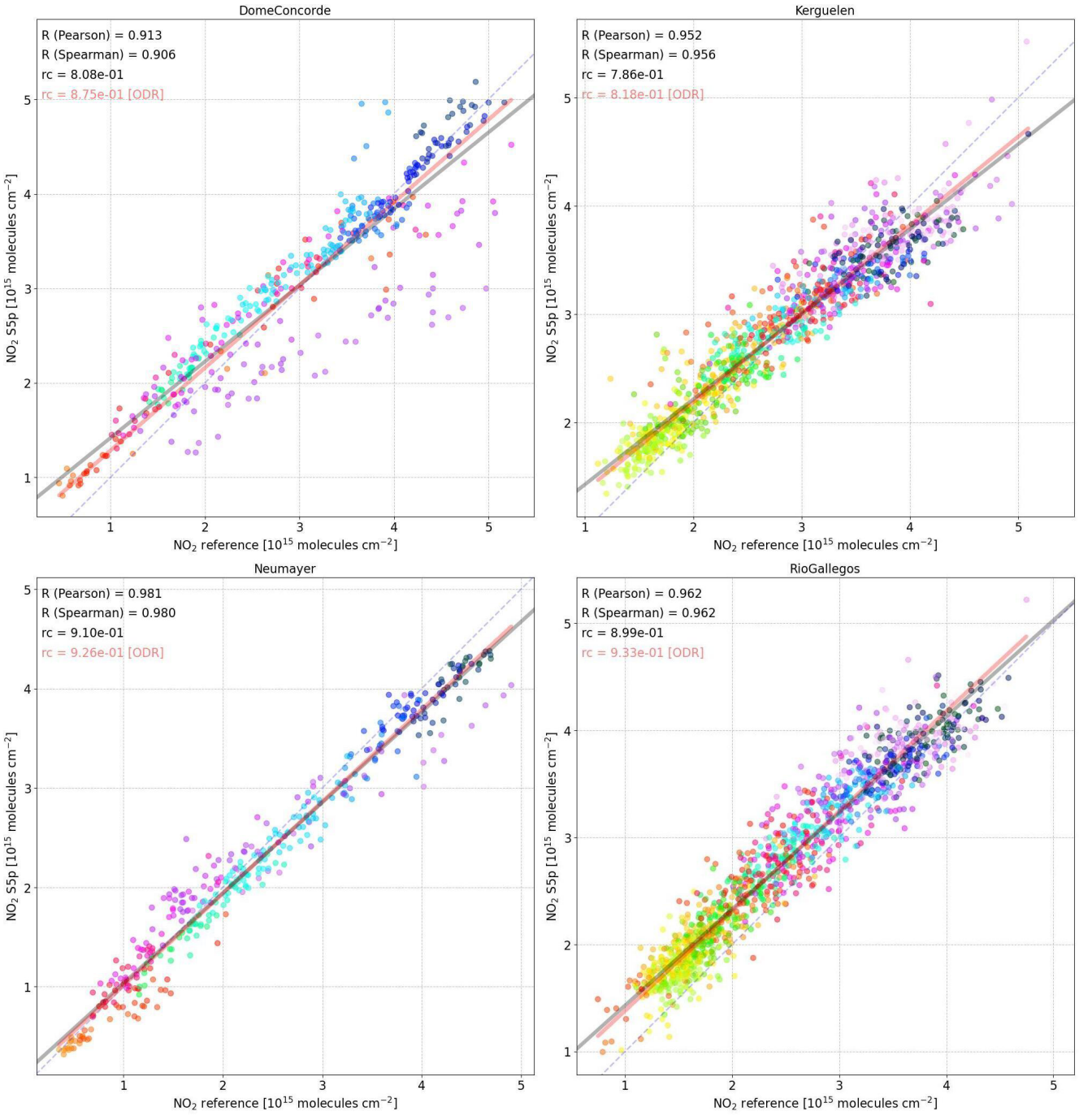

Figure A3. As Fig. 1b but for the other surface measurement stations in Table 1.

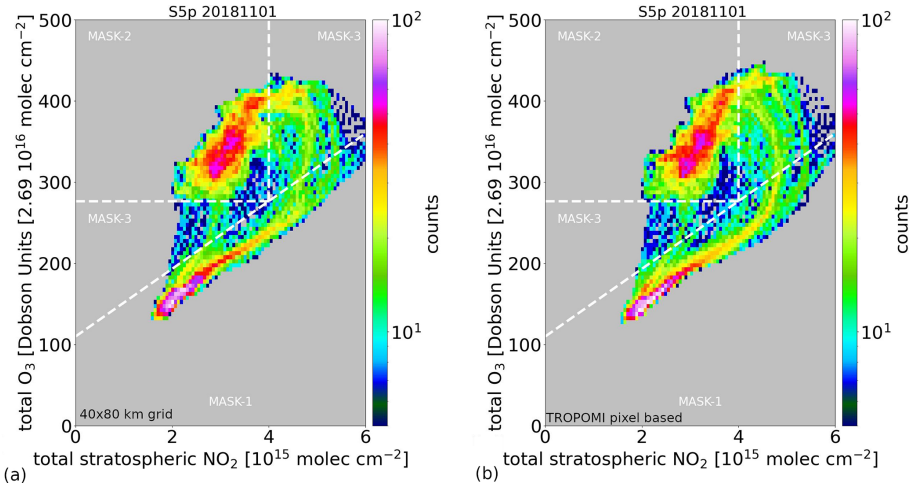

Figure A4. Comparison of 2D histograms of **(a)** TROPOMI SNO_2 data using the 40×80 km daily averages collocated with TCO_3 data (as Fig. 5a) and **(b)** TROPOMI SNO_2 pixel-level data collocated with TCO_3 data.

Data availability. TROPOMI NO_2 v2.3.1 intermediate S5P-PAL reprocessing data (Eskes et al., 2021b; last accessed 6 December 2022) used in this paper are no longer publicly accessible. They are superseded by the TROPOMI NO_2 Non Time Critical dataset (NTC; https://doi.org/10.5270/S5P-9bnp8q8, van Geffen et al., 2022b), available at https://dataspace.copernicus.eu/ (last access: December 2022). The TROPOMI NO_2 dataset used in this paper can still be made available on request. Multi-Sensor Reanalysis (MSR) gridded daily total ozone data are available via the TEMIS web portal (TCO_3; https://doi.org/10.21944/temis-ozone-msr2, Van der A et al., 2015b) and the TROPOMI validation data facility (SAOZ data and collocated TROPOMI TNO_2 and TROPOMI assimilated SNO_2; https://mpc-vdaf.tropomi.eu/index.php/nitrogen-dioxide, Sentinel-5P Validation Data Analysis Facility, 2022a; and https://mpc-vdaf-server.tropomi.eu/no2, Sentinel-5P Validation Data Analysis Facility, 2022b).

Supplement. The supplement related to this article is available online at: https://doi.org/10.5194/acp-24-4511-2024-supplement.

Author contributions. AdL wrote the paper and did the majority of the data analysis and interpretation. JvG did the data processing and also participated in the data analysis. PS is the instigator of this piece of research. JPV is the PI of Sentinel-5p/TROPOMI. HE is responsible for the TNO_2 data assimilation product, and RvdA maintains the TCO_3 data assimilation and data dissemination. All authors contributed to the discussion and interpretation of results.

Competing interests. The contact author has declared that none of the authors has any competing interests.

Disclaimer. Publisher's note: Copernicus Publications remains neutral with regard to jurisdictional claims made in the text, published maps, institutional affiliations, or any other geographical representation in this paper. While Copernicus Publications makes every effort to include appropriate place names, the final responsibility lies with the authors.

Acknowledgements. Sentinel-5 Precursor is a European Space Agency (ESA) mission on behalf of the European Commission (EC). The TROPOMI payload is a joint development by the ESA and the Netherlands Space Office (NSO). The Sentinel-5 Precursor ground-segment development has been funded by the ESA and with national contributions from the Netherlands, Germany, and Belgium. This work contains modified Copernicus Sentinel-5P TROPOMI data (2018–2022), processed in the operational framework or locally at KNMI. The authors thank the two referees and the editor for their valuable comments and suggestions that helped improve the paper.

Review statement. This paper was edited by Farahnaz Khosrawi and reviewed by Hideaki Nakajima and one anonymous referee.

References

Adams, C., Strong, K., Zhao, X., Bourassa, A. E., Daffer, W. H., Degenstein, D., Drummond, J. R., Farahani, E. E., Fraser, A., Lloyd, N. D., Manney, G. L., McLinden, C. A., Rex, M., Roth, C., Strahan, S. E., Walker, K. A., and Wohltmann, I.: The spring 2011 final stratospheric warming above Eureka: anomalous dynamics and chemistry, Atmos. Chem. Phys., 13, 611–624, https://doi.org/10.5194/acp-13-611-2013, 2013.

Appenzeller, C. and Holton, J. R.: Tracer lamination in the stratosphere: A global climatology, J. Geophys. Res., 102, 13555–13569, https://doi.org/10.1029/97JD00066, 1997.

Barbero, A., Savarino, J., Grilli, R., Blouzon, C., Picard, G., Frey, M. M., Huang, Y., and Caillon, N.: New estimation of the NO_x snow-source on the Antarctic Plateau, J. Geophys. Res.-Atmos., 126, e2021JD035062, https://doi.org/10.1029/2021JD035062, 2021.

Barré, J., Peuch, V.-H., Attié, J.-L., El Amraoui, L., Lahoz, W. A., Josse, B., Claeyman, M., and Nédélec, P.: Stratosphere-troposphere ozone exchange from high resolution MLS ozone analyses, Atmos. Chem. Phys., 12, 6129–6144, https://doi.org/10.5194/acp-12-6129-2012, 2012.

Beirle, S., Hörmann, C., Jöckel, P., Liu, S., Penning de Vries, M., Pozzer, A., Sihler, H., Valks, P., and Wagner, T.: The STRatospheric Estimation Algorithm from Mainz (STREAM): estimating stratospheric NO_2 from nadir-viewing satellites by weighted convolution, Atmos. Meas. Tech., 9, 2753–2779, https://doi.org/10.5194/amt-9-2753-2016, 2016.

Belmonte Rivas, M., Veefkind, P., Boersma, F., Levelt, P., Eskes, H., and Gille, J.: Intercomparison of daytime stratospheric NO_2 satellite retrievals and model simulations, Atmos. Meas. Tech., 7, 2203–2225, https://doi.org/10.5194/amt-7-2203-2014, 2014.

Bodeker, G. E., Struthers, H., and Connor, B. J.: Dynamical containment of Antartic ozone depletion, Geophys. Res. Lett., 29, 1098, https://doi.org/10.1029/2001GL014206, 2002.

Boersma, K. F., Eskes, H. J., and Brinksma, E. J.: Error analysis for tropospheric NO_2 retrieval from space, J. Geophys. Res., 109, D04311, https://doi.org/10.1029/2003JD003962, 2004.

Boersma, K. F., Eskes, H. J., Veefkind, J. P., Brinksma, E. J., van der A, R. J., Sneep, M., van den Oord, G. H. J., Levelt, P. F., Stammes, P., Gleason, J. F., and Bucsela, E. J.: Near-real time retrieval of tropospheric NO_2 from OMI, Atmos. Chem. Phys., 7, 2103–2118, https://doi.org/10.5194/acp-7-2103-2007, 2007.

Boersma, K. F., Eskes, H. J., Dirksen, R. J., van der A, R. J., Veefkind, J. P., Stammes, P., Huijnen, V., Kleipool, Q. L., Sneep, M., Claas, J., Leitão, J., Richter, A., Zhou, Y., and Brunner, D.: An improved tropospheric NO_2 column retrieval algorithm for the Ozone Monitoring Instrument, Atmos. Meas. Tech., 4, 1905–1928, https://doi.org/10.5194/amt-4-1905-2011, 2011.

Boersma, K. F., Eskes, H. J., Richter, A., De Smedt, I., Lorente, A., Beirle, S., van Geffen, J. H. G. M., Zara, M., Peters, E., Van Roozendael, M., Wagner, T., Maasakkers, J. D., van der A, R. J., Nightingale, J., De Rudder, A., Irie, H., Pinardi, G., Lambert, J.-C., and Compernolle, S. C.: Improving algorithms and uncertainty estimates for satellite NO_2 retrievals: results from the quality assurance for the essential climate variables (QA4ECV) project, Atmos. Meas. Tech., 11, 6651–6678, https://doi.org/10.5194/amt-11-6651-2018, 2018.

Bortoli, D., Giovanelli, G., Ravegnani, F., Kostadinov, I., and Petritoli, A.: Stratospheric nitrogen dioxide in the Antarctic, Int. J. Remote Sens., 26, 3395–3412, https://doi.org/10.1080/01431160500076418, 2005.

Bortoli, D., Ravegnani, F., Giovanelli, G., Kulkarni, P. S., Anton, M., Costa, M. J., and Silva, A. M.: Fifteen years of stratospheric nitrogen dioxide and ozone measurements in Antarctica, AIP Conf. Proc., 1531, 300–303, https://doi.org/10.1063/1.4804766, 2013.

Bourassa, A. E., McLinden, C. A., Sioris, C. E., Brohede, S., Bathgate, A. F., Llewellyn, E. J., and Degenstein, D. A.: Fast NO_2 retrievals from Odin-OSIRIS limb scatter measurements, Atmos. Meas. Tech., 4, 965–972, https://doi.org/10.5194/amt-4-965-2011, 2011.

Butler, A. H. and Domeisen, D. I. V.: The wave geometry of final stratospheric warming events, Weather Clim. Dynam., 2, 453–474, https://doi.org/10.5194/wcd-2-453-2021, 2021.

Butz, A., Bösch, H., Camy-Peyret, C., Chipperfield, M., Dorf, M., Dufour, G., Grunow, K., Jeseck, P., Kühl, S., Payan, S., Pepin, I., Pukite, J., Rozanov, A., von Savigny, C., Sioris, C., Wagner, T., Weidner, F., and Pfeilsticker, K.: Inter-comparison of stratospheric O_3 and NO_2 abundances retrieved from balloon borne direct sun observations and Envisat/SCIAMACHY limb measurements, Atmos. Chem. Phys., 6, 1293–1314, https://doi.org/10.5194/acp-6-1293-2006, 2006.

Callis, L. B., Russell III, J. M., Haggard, K. V., and Natarajan, M.: Examination of wintertime latitudinal gradients in stratospheric NO_2 using theory and LIMS observations, Geophys. Res. Lett., 10, 945–948, https://doi.org/10.1029/GL010i010p00945, 1983.

Compernolle, S., Verhoelst, T., Pinardi, G., Granville, J., Hubert, D., Keppens, A., Niemeijer, S., Rino, B., Bais, A., Beirle, S., Boersma, F., Burrows, J. P., De Smedt, I., Eskes, H., Goutail, F., Hendrick, F., Lorente, A., Pazmino, A., Piters, A., Peters, E., Pommereau, J.-P., Remmers, J., Richter, A., van Geffen, J., Van Roozendael, M., Wagner, T., and Lambert, J.-C.: Validation of Aura-OMI QA4ECV NO_2 climate data records with ground-based DOAS networks: the role of measurement and comparison uncertainties, Atmos. Chem. Phys., 20, 8017–8045, https://doi.org/10.5194/acp-20-8017-2020, 2020.

Cook, P. A. and Roscoe, H. K.: Variability and trends in stratospheric NO_2 in Antarctic summer, and implications for stratospheric NO_y, Atmos. Chem. Phys., 9, 3601–3612, https://doi.org/10.5194/acp-9-3601-2009, 2009.

Davies, S., Mann, G. W., Carslaw, K. S., Chipperfield, M. P., Remedios, J. J., Allen, G., Waterfall, A. M., Spang, R., and Toon, G. C.: Testing our understanding of Arctic denitrification using MIPAS-E satellite measurements in winter 2002/2003, Atmos. Chem. Phys., 6, 3149–3161, https://doi.org/10.5194/acp-6-3149-2006, 2006.

de Laat, A. and van Weele, M.: The 2010 Antarctic ozone hole: Observed reduction in ozone destruction by minor sudden stratospheric warmings, Sci. Rep., 1, 38, https://doi.org/10.1038/srep00038, 2011.

de Leeuw, J., Schmidt, A., Witham, C. S., Theys, N., Taylor, I. A., Grainger, R. G., Pope, R. J., Haywood, J., Osborne, M., and Kristiansen, N. I.: The 2019 Raikoke volcanic eruption – Part 1: Dispersion model simulations and satellite retrievals of volcanic sulfur dioxide, Atmos. Chem. Phys., 21, 10851–10879, https://doi.org/10.5194/acp-21-10851-2021, 2021.

Dessler, A.: Chemistry and Physics of Stratospheric Ozone, Elsevier, ISBN 9780080500966, 2000.

Dirksen, R. J., Boersma, K. F., Eskes, H. J., Ionov, D. V., Bucsela, E. J., Levelt, P. F., and Kelder, H. M.: Evaluation of stratospheric NO_2 retrieved from the Ozone Monitoring Instrument: Intercomparison, diurnal cycle, and trending, J. Geophys. Res. 116, D08305, https://doi.org/10.1029/2010JD014943, 2011.

Dubé, K., Randel, W., Bourassa, A., Zawada, D., McLinden, C., and Degenstein, D.: Trends and variability in stratospheric

NO_x derived from merged SAGE II and OSIRIS satellite observations, J. Geophys. Res.-Atmos., 125, e2019JD031798, https://doi.org/10.1029/2019JD031798, 2020.

Dubé, K., Bourassa, A., Zawada, D., Degenstein, D., Damadeo, R., Flittner, D., and Randel, W.: Accounting for the photochemical variation in stratospheric NO_2 in the SAGE III/ISS solar occultation retrieval, Atmos. Meas. Tech., 14, 557–566, https://doi.org/10.5194/amt-14-557-2021, 2021.

Errera, Q. and Fonteyn, D.: Four-dimensional variational chemical assimilation of CRISTA stratospheric measurements, J. Geophys. Res., 106, 12253–12265, https://doi.org/10.1029/2001JD900010, 2001.

Eskes, H., van Velthoven, P., Valks, P., and Kelder, H.: Assimilation of GOME total ozone satellite observations in a three-dimensional tracer transport model, Q. J. Roy. Meteor. Soc. 129, 1663–1681, https://doi.org/10.1256/qj.02.14, 2003.

Eskes, H. J. and Eichmann, K.-U.: S5P MPC Product Readme Nitrogen Dioxide, Report S5P-MPC-KNMI-PRF-NO_2, version 2.2, 2022-07-20, ESA, http://www.tropomi.eu/data-products/nitrogen-dioxide/ (last access: 6 December 2022), 2022.

Eskes, H., van Geffen, J., Sneep, M., Veefkind, P., Niemeijer, S., and Zehner, C.: S5P Nitrogen Dioxide v02.03.01 intermediate reprocessing on the S5P-PAL system: Readme file Report, version 1.0, 2021-12-15, ESA, https://data-portal.s5p-pal.com/product-docs/no2/PAL_reprocessing_NO2_v02.03.01_20211215.pdf (last access: 6 December 2022), 2021a.

Eskes, H. J., van Geffen, J. H. G. M., Boersma, K. F., Eichmann K.-U.. Apituley, A., Pedergnana, M., Sneep, M., Veefkind, J. P., and Loyola, D.: S5P/TROPOMI Level-2 Product User Manual Nitrogen Dioxide, Report S5P-KNMI-L2-0021-MA, version 4.0.2, ESA, https://sentinel.esa.int/documents/247904/2474726/Sentinel-5P-Level-2-Product-User-Manual-Nitrogen-Dioxide.pdf (last access: 6 December 2021), 2021b.

Fahey, D., Solomon, S., Kawa, S., Lowenstein, M., Podolske, J. J., Strahan, S. E., and Chan, K. R.: A diagnostic for denitrification in the winter polar stratospheres, Nature, 345, 698–702, https://doi.org/10.1038/345698a0, 1990.

Fahey, D. W., Murphy, D. M., Kelly, K. K., Ko, M. K. W., Proffitt, M. H., Eubank, C. S., Ferry, G. V., Loewenstein, M., and Chan, K. R.: Measurements of nitric oxide and total reactive nitrogen in the Antarctic stratosphere: Observations and chemical implications, J. Geophys. Res., 94, 16665–16681, https://doi.org/10.1029/JD094iD14p16665, 1989.

Farman, J., Gardiner, B., and Shanklin, J.: Large losses of total ozone in Antarctica reveal seasonal ClO_x / NO_x interaction, Nature, 315, 207–210, https://doi.org/10.1038/315207a0, 1985.

France, J. L., King, M. D., Frey, M. M., Erbland, J., Picard, G., Preunkert, S., MacArthur, A., and Savarino, J.: Snow optical properties at Dome C (Concordia), Antarctica; implications for snow emissions and snow chemistry of reactive nitrogen, Atmos. Chem. Phys., 11, 9787–9801, https://doi.org/10.5194/acp-11-9787-2011, 2011.

Frey, M. M., Brough, N., France, J. L., Anderson, P. S., Traulle, O., King, M. D., Jones, A. E., Wolff, E. W., and Savarino, J.: The diurnal variability of atmospheric nitrogen oxides (NO and NO_2) above the Antarctic Plateau driven by atmospheric stability and snow emissions, Atmos. Chem. Phys., 13, 3045–3062, https://doi.org/10.5194/acp-13-3045-2013, 2013.

Frey, M. M., Roscoe, H. K., Kukui, A., Savarino, J., France, J. L., King, M. D., Legrand, M., and Preunkert, S.: Atmospheric nitrogen oxides (NO and NO_2) at Dome C, East Antarctica, during the OPALE campaign, Atmos. Chem. Phys., 15, 7859–7875, https://doi.org/10.5194/acp-15-7859-2015, 2015.

Funke, B., López-Puertas, M., Gil-López, S., von Clarmann, T., Stiller, G. P., Fischer, H., and Kellmann, S.: Downward transport of upper atmospheric NO_x into the polar stratosphere and lower mesosphere during the Antarctic 2003 and Arctic 2002/2003 winters, J. Geophys. Res., 110, D24308, https://doi.org/10.1029/2005JD006463, 2005.

Garcia, R. R. and Solomon, S.: A new numerical model of the middle atmosphere: 2. Ozone and related species, J. Geophys. Res., 99, 12937–12951, https://doi.org/10.1029/94JD00725, 1994.

Gil, M. and Cacho, J.: NO_2 total column evolution during the 1989 spring at Antarctica Peninsula, J. Atmos. Chem., 15, 187–200, https://doi.org/10.1007/BF00053759, 1992.

Goldman, A., Fernald, F. A., Williams, W. J., and Murcray, D. G.: Vertical distribution of NO_2 in the stratosphere as determined from balloon measurements of solar spectra in the 4500 Å region, Geophys. Res. Lett., 5, 257–260, https://doi.org/10.1029/GL005i004p00257, 1978.

Gordon, E. M., Seppälä, A., and Tamminen, J.: Evidence for energetic particle precipitation and quasi-biennial oscillation modulations of the Antarctic NO_2 springtime stratospheric column from OMI observations, Atmos. Chem. Phys., 20, 6259–6271, https://doi.org/10.5194/acp-20-6259-2020, 2020.

Haley, C., Brohede, S., Sioris, C., Griffioen, E., Murtagh, D., Mcdade, I., Eriksson, P., Llewellyn, E., Bazureau, A., and Goutail, F.: Retrieval of stratospheric O_3 and NO_2 profiles from Odin Optical Spectrograph and Infrared Imager System (OSIRIS) limb-scattered sunlight measurements, J. Geophys. Res., 109, D16303, https://doi.org/10.1029/2004JD004588, 2004.

Hendrick, F., Barret, B., Van Roozendael, M., Boesch, H., Butz, A., De Mazière, M., Goutail, F., Hermans, C., Lambert, J.-C., Pfeilsticker, K., and Pommereau, J.-P.: Retrieval of nitrogen dioxide stratospheric profiles from ground-based zenith-sky UV-visible observations: validation of the technique through correlative comparisons, Atmos. Chem. Phys., 4, 2091–2106, https://doi.org/10.5194/acp-4-2091-2004, 2004.

Hendrick, F., Pommereau, J.-P., Goutail, F., Evans, R. D., Ionov, D., Pazmino, A., Kyrö, E., Held, G., Eriksen, P., Dorokhov, V., Gil, M., and Van Roozendael, M.: NDACC/SAOZ UV-visible total ozone measurements: improved retrieval and comparison with correlative ground-based and satellite observations, Atmos. Chem. Phys., 11, 5975–5995, https://doi.org/10.5194/acp-11-5975-2011, 2011.

Hilboll, A., Richter, A., Rozanov, A., Hodnebrog, Ø., Heckel, A., Solberg, S., Stordal, F., and Burrows, J. P.: Improvements to the retrieval of tropospheric NO_2 from satellite – stratospheric correction using SCIAMACHY limb/nadir matching and comparison to Oslo CTM2 simulations, Atmos. Meas. Tech., 6, 565–584, https://doi.org/10.5194/amt-6-565-2013, 2013.

Hoffmann, L., Hertzog, A., Rößler, T., Stein, O., and Wu, X.: Intercomparison of meteorological analyses and trajectories in the Antarctic lower stratosphere with Concordiasi superpressure balloon observations, Atmos. Chem. Phys., 17, 8045–8061, https://doi.org/10.5194/acp-17-8045-2017, 2017.

Hoor, P., Fischer, H., Lange, L., Lelieveld, J., and Brunner, D.: Seasonal variations of a mixing layer in the lowermost stratosphere as identified by the CO-O_3 correlation from in situ measurements, J. Geophys. Res., 107, 4044, https://doi.org/10.1029/2000JD000289, 2002.

Hurwitz, M. M., Fleming, E. L., Newman, P. A., Li, F., Mlawer, E., Cady-Pereira, K., and Bailey, R.: Ozone depletion by hydrofluorocarbons, Geophys. Res. Lett., 42, 8686–8692, https://doi.org/10.1002/2015GL065856, 2015.

Joseph, B., and Legras, B.: Relation between Kinematic Boundaries, Stirring, and Barriers for the Antarctic Polar Vortex, J. Atmos. Sci., 59, 1198–1212, https://doi.org/10.1175/1520-0469(2002)059<1198:RBKBSA>2.0.CO;2, 2002.

Kerzenmacher, T., Wolff, M. A., Strong, K., Dupuy, E., Walker, K. A., Amekudzi, L. K., Batchelor, R. L., Bernath, P. F., Berthet, G., Blumenstock, T., Boone, C. D., Bramstedt, K., Brogniez, C., Brohede, S., Burrows, J. P., Catoire, V., Dodion, J., Drummond, J. R., Dufour, D. G., Funke, B., Fussen, D., Goutail, F., Griffith, D. W. T., Haley, C. S., Hendrick, F., Höpfner, M., Huret, N., Jones, N., Kar, J., Kramer, I., Llewellyn, E. J., López-Puertas, M., Manney, G., McElroy, C. T., McLinden, C. A., Melo, S., Mikuteit, S., Murtagh, D., Nichitiu, F., Notholt, J., Nowlan, C., Piccolo, C., Pommereau, J.-P., Randall, C., Raspollini, P., Ridolfi, M., Richter, A., Schneider, M., Schrems, O., Silicani, M., Stiller, G. P., Taylor, J., Tétard, C., Toohey, M., Vanhellemont, F., Warneke, T., Zawodny, J. M., and Zou, J.: Validation of NO_2 and NO from the Atmospheric Chemistry Experiment (ACE), Atmos. Chem. Phys., 8, 5801–5841, https://doi.org/10.5194/acp-8-5801-2008, 2008.

Khaykin, S., Legras, B., Bucci, S., Sellitto, P., Isaksen, L., Tencé, F., Bekki, S., Bourassa, A., Rieger, L., Zawada, D., Jumelet, J., and Godin-Beekmann, S.: The 2019/20 Australian wildfires generated a persistent smoke-charged vortex rising up to 35 km altitude, Commun. Earth Environ., 1, 1–12, https://doi.org/10.1038/s43247-020-00022-5, 2020.

Khaykin, S. M., de Laat, A. T. J., Godin-Beekmann, S.. Hauchecorne, A., and M. Ratynski: Unexpected self-lofting and dynamical confinement of volcanic plumes: the Raikoke 2019 case, Sci. Rep., 12, 22409, https://doi.org/10.1038/s41598-022-27021-0, 2022.

Khosrawi, F., Urban, J., Pitts, M. C., Voelger, P., Achtert, P., Kaphlanov, M., Santee, M. L., Manney, G. L., Murtagh, D., and Fricke, K.-H.: Denitrification and polar stratospheric cloud formation during the Arctic winter 2009/2010, Atmos. Chem. Phys., 11, 8471–8487, https://doi.org/10.5194/acp-11-8471-2011, 2011.

Khosrawi, F., Kirner, O., Sinnhuber, B.-M., Johansson, S., Höpfner, M., Santee, M. L., Froidevaux, L., Ungermann, J., Ruhnke, R., Woiwode, W., Oelhaf, H., and Braesicke, P.: Denitrification, dehydration and ozone loss during the 2015/2016 Arctic winter, Atmos. Chem. Phys., 17, 12893–12910, https://doi.org/10.5194/acp-17-12893-2017, 2017.

Koh, T. Y. and Legras, B.: Hyperbolic lines and the stratospheric polar vortex, Chaos, 12, 382–394, https://doi.org/10.1063/1.1480442, 2002.

Kondo, Y., Matthews, W. A., Solomon, S., Koike, M., Hayashi, M., Yamazaki, K., Nakajima, H., and Tsukui, K.: Ground-based measurements of column amounts of NO_2 over Syowa Station, Antarctica, J. Geophys. Res., 99, 14535–14548, https://doi.org/10.1029/94JD00403, 1994.

Krasauskas, L., Ungermann, J., Preusse, P., Friedl-Vallon, F., Zahn, A., Ziereis, H., Rolf, C., Plöger, F., Konopka, P., Vogel, B., and Riese, M.: 3-D tomographic observations of Rossby wave breaking over the North Atlantic during the WISE aircraft campaign in 2017, Atmos. Chem. Phys., 21, 10249–10272, https://doi.org/10.5194/acp-21-10249-2021, 2021.

Kritten, L., Butz, A., Dorf, M., Deutschmann, T., Kühl, S., Prados-Roman, C., Puķīte, J., Rozanov, A., Schofield, R., and Pfeilsticker, K.: Time dependent profile retrieval of UV/vis absorbing radicals from balloon-borne limb measurements – a case study on NO_2 and O_3, Atmos. Meas. Tech., 3, 933–946, https://doi.org/10.5194/amt-3-933-2010, 2010.

Krotkov, N., Realmuto, V., Li, C., Seftor, C., Li, J., Brentzel, K., Stuefer, M., Cable, J., Dierking, C., Delamere, J., Schneider, D., Tamminen, J., Hassinen, S., Ryyppö, T., Murray, J., Carn, S., Osiensky, J., Eckstein, N., Layne, G., and Kirkendall, J.: Day–Night Monitoring of Volcanic SO_2 and Ash Clouds for Aviation Avoidance at Northern Polar Latitudes, Remote Sensi., 13, 4003, https://doi.org/10.3390/rs13194003, 2021.

Kühl, S., Wilms-Grabe, W., Frankenberg, C., Grzegorski, M., Platt, U., and Wagner, T.: Comparison of OClO nadir measurements from SCIAMACHY and GOME, Adv. Space Res., 37, 2247–2253, https://doi.org/10.1016/j.asr.2005.06.061, 2006.

Kühl, S., Pukite, J., Deutschmann, T., Platt, U., and Wagner, T.: SCIAMACHY limb measurements of NO_2, BrO and OClO. Retrieval of vertical profiles: Algorithm, first results, sensitivity and comparison studies, Adv. Space Res., 42, 1747–1764, 2008.

Lambert, J.-C., Compernolle, S., Eichmann, K.-U., de Graaf, M., Hubert, D., Keppens, A., Kleipool, Q., Langerock, B., Sha, M. K., Verhoelst, T., Wagner, T., Ahn, C., Argyrouli, A., Balis, D., Chan, K. L., De Smedt, I., Eskes, H., Fjæraa, A. M., Garane, K., Gleason, J. F., Goutail, F., Granville, J., Hedelt, P., Heue, K.-P., Jaross, G., Koukouli, M.-L., Landgraf, J., Lutz, R., Nanda, S., Niemeijer, S., Pazmiño, A., Pinardi, G., Pommereau, J.-P., Richter, A., Rozemeijer, N., Sneep, M., Stein Zweers, D., Theys, N., Tilstra, G., Torres, O., Valks, P., van Geffen, J., Vigouroux, C., Wang, P., and Weber, M.: Quarterly Validation Report of the Copernicus Sentinel-5 Precursor Operational Data Products, #16: April 2018–August 2022, S5P MPC Routine Operations Consolidated Validation Report series, Issue 16.01.00, 189 pp., 2022-09-23, https://mpc-vdaf.tropomi.eu/ProjectDir/reports/pdf/S5P-MPC-IASB-ROCVR-16.01.00-20220923.pdf (last access: June 2023), 2023.

Lecouffe, A., Godin-Beekmann, S., Pazmiño, A., and Hauchecorne, A.: Evolution of the intensity and duration of the Southern Hemisphere stratospheric polar vortex edge for the period 1979–2020, Atmos. Chem. Phys., 22, 4187–4200, https://doi.org/10.5194/acp-22-4187-2022, 2022.

Lindenmaier, R., Strong, K., Batchelor, R. L., Bernath, P. F., Chabrillat, S., Chipperfield, M. P., Daffer, W. H., Drummond, J. R., Feng, W., Jonsson, A. I., Kolonjari, F., Manney, G. L., McLinden, C., Ménard, R., and Walker, K. A.: A study of the Arctic NOy budget above Eureka, Canada, J. Geophys. Res., 116, D23302, https://doi.org/10.1029/2011JD016207, 2011.

Magaritz-Ronen, L. and Raveh-Rubin, S.: Wildfire smoke highlights troposphere-to-stratosphere pathway, Geophys. Res. Lett.,

48, e2021GL095848, https://doi.org/10.1029/2021GL095848, 2021.

Maliniemi, V., Nesse Tyssøy, H., Smith-Johnsen, C., Arsenovic, P., and Marsh, D. R.: Effects of enhanced downwelling of NO_x on Antarctic upper-stratospheric ozone in the 21st century, Atmos. Chem. Phys., 21, 11041–11052, https://doi.org/10.5194/acp-21-11041-2021, 2021.

Manney, G. L., Santee, M. L., Livesey, N. J., Froidevaux, L., Read, W. G., Pumphrey, H. C., Waters, J. W., and Pawson, S.: EOS Microwave Limb Sounder observations of the Antarctic polar vortex breakup in 2004, Geophys. Res. Lett., 32, L12811, https://doi.org/10.1029/2005GL022823, 2005.

Mount, G. H., Rusch, D. W., Noxon, J. F., Zawodny, J. M., and Barth, C. A.: Measurements of stratospheric NO_2 from the Solar Mesosphere Explorer satellite: 1. An overview of the results, J. Geophys. Res., 89, 1327–1340, https://doi.org/10.1029/JD089iD01p01327, 1984.

Müller, R.: The impact of the rise in atmospheric nitrous oxide on stratospheric ozone, Ambio, 50, 35–39, https://doi.org/10.1007/s13280-020-01428-3, 2021.

Müller, R., Grooß, J.-U., Lemmen, C., Heinze, D., Dameris, M., and Bodeker, G.: Simple measures of ozone depletion in the polar stratosphere, Atmos. Chem. Phys., 8, 251–264, https://doi.org/10.5194/acp-8-251-2008, 2008.

Munro, R., Eisinger, M., Anderson, C., Callies, J., Corpaccioli, E., Lang, R., Lefebvre, A., Livschitz, Y., and Albinana, A. P.: GOME-2 on MetOp, Proceedings of the 2006 EUMETSAT Meteorological Satellite Conference, 12–16 June 2006, Helsinki, Finland, Vol. 1216, ESA publication SP 628, Paris, France, ISBN 92-9110-076-5, 2006.

Munro, R., Lang, R., Klaes, D., Poli, G., Retscher, C., Lindstrot, R., Huckle, R., Lacan, A., Grzegorski, M., Holdak, A., Kokhanovsky, A., Livschitz, J., and Eisinger, M.: The GOME-2 instrument on the Metop series of satellites: instrument design, calibration, and level 1 data processing – an overview, Atmos. Meas. Tech., 9, 1279–1301, https://doi.org/10.5194/amt-9-1279-2016, 2016.

Newman, P. A., Lait, L. R., Schoeberl, M. R., Seablom, M., Coy, L., Rood, R., Swinbank, R., Proffitt, M., Loewenstein, M., Podolske, J. R., Elkins, J. W., Webster, C. R., May, R. D., Fahey, D. W., Dutton, G. S., and Chan, K. R., Measurements of polar vortex air in the midlatitudes, J. Geophys. Res., 101, 12879 https://doi.org/10.1029/95JD03387, 1996.

Noxon, J. F.: Stratospheric NO_2 in the Antarctic winter, Geophys. Res. Lett., 5, 1021–1022, https://doi.org/10.1029/GL005i012p01021, 1978.

Noxon, J. F.: Stratospheric NO_2: 2. Global behavior, J. Geophys. Res., 84, 5067–5076, https://doi.org/10.1029/JC084iC08p05067, 1979.

Oetjen, H., Wittrock, F., Richter, A., Chipperfield, M. P., Medeke, T., Sheode, N., Sinnhuber, B.-M., Sinnhuber, M., and Burrows, J. P.: Evaluation of stratospheric chlorine chemistry for the Arctic spring 2005 using modelled and measured OClO column densities, Atmos. Chem. Phys., 11, 689–703, https://doi.org/10.5194/acp-11-689-2011, 2011.

Oppenheimer, C., Kyle, P. R., Tsanev, V. I., McGonigle, A. J. S., Mather, T. A., and Sweeney, D.: Mt. Erebus, the largest point source of NO_2 in Antarctica, Atmos. Environ., 39, 6000–6006, https://doi.org/10.1016/j.atmosenv.2005.06.036, 2005.

Orsolini, Y. J. and Grant, W. B.: Seasonal formation of nitrous oxide laminae in the mid and low latitude stratosphere, Geophys. Res. Lett., 27, 1119–1122, https://doi.org/10.1029/95JD03387, 2000.

Pinardi, G., Van Roozendael, M., Hendrick, F., Richter, A., Valks, P., Alwarda, R., Bognar, K., Frieß, U., Granville, J., Gu, M., Johnston, P., Prados-Roman, C., Querel, R., Strong, K., Wagner, T., Wittrock, F., and Yela Gonzalez, M.: Ground-based validation of the MetOp-A and MetOp-B GOME-2 OClO measurements, Atmos. Meas. Tech., 15, 3439–3463, https://doi.org/10.5194/amt-15-3439-2022, 2022.

Plumb, R. A.: Tracer interrelationships in the stratosphere, Rev. Geophys., 45, RG4005, https://doi.org/10.1029/2005RG000179, 2007.

Pommereau, J. P. and Goutail, F.: O_3 and NO_2 ground-based measurements by visible spectrometry during Arctic winter and spring 1988, Geophys. Res. Lett., 15, 891–894, https://doi.org/10.1029/GL015i008p00891, 1988.

Puķīte, J., Borger, C., Dörner, S., Gu, M., Frieß, U., Meier, A. C., Enell, C.-F., Raffalski, U., Richter, A., and Wagner, T.: Retrieval algorithm for OClO from TROPOMI (TROPOspheric Monitoring Instrument) by differential optical absorption spectroscopy, Atmos. Meas. Tech., 14, 7595–7625, https://doi.org/10.5194/amt-14-7595-2021, 2021.

Ricaud, P., Lefèvre, F., Berthet, G., Murtagh, D., Llewellyn, E. J., Mégie, G., Kyrölä, E., Leppelmeier, G. W., Auvinen, H., Boonne, C., Brohede, S., Degenstein, D. A., de La Noë, J., Dupuy, E., El Amraoui, L., Eriksson, P., Evans, W. F. J., Frisk, U., Gattinger, R. L., Girod, F., Haley, C. S., Hassinen, S., Hauchecorne, A., Jimenez, C., Kyrö, E., Lautié, N., Le Flochmoën, E., Lloyd, N. D., McConnell, J. C., McDade, I. C., Nordh, L., Olberg, M., Pazmino, A., Petelina, S. V., Sandqvist, A., Seppälä, A., Sioris, C. E., Solheim, B. H., Stegman, J., Strong, K., Taalas, P., Urban, J., von Savigny, C., von Scheele, F., and Witt, G.: Polar vortex evolution during the 2002 Antarctic major warming as observed by the Odin satellite, J. Geophys. Res., 110, D05302, https://doi.org/10.1029/2004JD005018, 2005.

Richter, A., Wittrock, F., Weber, M., Beirle, S., Kühl, S., Platt, U., Wagner, T., Wilms-Grabe, W., and Burrows, J. P.: GOME observations of stratospheric trace gas distributions during the splitting vortex event in the Antarctic winter of 2002. Part I: Measurements, J. Atmos. Sci., 62, 778–785, https://doi.org/10.1175/JAS-3325.1, 2005.

Ridley, B. A., Luu, S. H., Hastie, D. R., Schiff, H. I., McConnell, J. C., Evans, W. F. J., McElroy, C. T., Kerr, J. B., Fast, H., and O'Brien, R. S.: Stratospheric odd nitrogen: Measurements of HNO_3, NO, NO_2, and O_3 near 54° N in winter, J. Geophys. Res., 89, 4797–4820, https://doi.org/10.1029/JD089iD03p04797, 1984.

Rinsland, C. P., Gunson, M. R., Salawitch, R. J., Michelsen, H. A., Zander, R., Newchurch, M. J., Abbas, M. M., Abrams, M. C., Manney, G. L., Chang, A. Y., Irion, F. W., Goldman, A., and Mahieu, E.: ATMOS/ATLAS-3 measurements of stratospheric chlorine and reactive nitrogen partitioning inside and outside the November 1994 Antarctic vortex. Geophys. Res. Lett., 23, 2365–2368, https://doi.org/10.1029/96GL01474, 1996.

Ronsmans, G., Langerock, B., Wespes, C., Hannigan, J. W., Hase, F., Kerzenmacher, T., Mahieu, E., Schneider, M., Smale, D., Hurtmans, D., De Mazière, M., Clerbaux, C., and Coheur, P.-F.: First characterization and validation of FORLI-HNO_3 verti-

cal profiles retrieved from IASI/Metop, Atmos. Meas. Tech., 9, 4783–4801, https://doi.org/10.5194/amt-9-4783-2016, 2016.

Russell, J. M., Solomon, S., Gordley, L. L., Remsberg, E. E., and Callis, L. B.: The variability of stratospheric and mesospheric NO_2 in the polar winter night observed by LIMS, J. Geophys. Res., 89, 7267–7275, https://doi.org/10.1029/JD089iD05p07267, 1984.

Safieddine, S., Bouillon, M., Paracho, A. C., Jumelet, J., Tence, F., Pazmino, A., Goutail, F., Wespes, C., Bekki, S., Boynard, A., Hadji-Lazaro, J., Coheur, P. F., Hurtmans, D., and Clerbaux, C.: Antarctic ozone enhancement during the 2019 sudden stratospheric warming event, Geophys. Res. Lett., 47, e2020GL087810, https://doi.org/10.1029/2020gl087810, 2020.

Salawitch, R., Gobbi, G., Wofsy, S., and McElroy, M. B.: Denitrification in the Antarctic stratosphere, Nature, 339, 525–527, https://doi.org/10.1038/339525a0, 1989.

Sanders, R. W., Solomon, S., Kreher, K., and Johnston, P. V.: An Intercomparison of NO_2 and OClO Measurements at Arrival Heights, Antarctica during Austral Spring 1996, J. Atmos. Chem., 33, 283–298, https://doi.org/10.1023/A:1006185027584, 1999.

Santee, M. L., MacKenzie, I. A., Manney, G. L., Chipperfield, M. P., Bernath, P. F., Walker, K. A., Boone, C. D., Froidevaux, L., Livesey, N. J., and Waters, J. W.: A study of stratospheric chlorine partitioning based on new satellite measurements and modeling, J. Geophys. Res., 113, D12307, https://doi.org/10.1029/2007JD009057, 2008.

Sato, K., Tomikawa, Y., Hashida, G., Yamanouchi, T., Nakajima, H., and Sugita, T.: Longitudinally Dependent Ozone Increase in the Antarctic Polar Vortex Revealed by Balloon and Satellite Observations, J. Atmos. Sci., 66, 1807–1820, https://doi.org/10.1175/2008JAS2904.1, 2009.

Schoeberl, M. R., Lait, L. R., Newman, P. A., and Rosenfield, J. E.: The structure of the polar vortex, J. Geophys. Res., 97, 7859–7882, https://doi.org/10.1029/91JD02168, 1992.

Sentinel-5P Validation Data Analysis Facility: Nitrogen Dioxide, Sentinel-5P VDAF [data set], https://mpc-vdaf.tropomi.eu/index.php/nitrogen-dioxide, last access: 12 November 2022a.

Sentinel-5P Validation Data Analysis Facility: NO_2 validations, Sentinel-5P MPC Validation Server [data set], https://mpc-vdaf-server.tropomi.eu/no2, last access: 12 November 2022b.

Smale, D., Strahan, S. E., Querel, R., Frieß, U., Nedoluha, G. E., Nichol, S. E., Robinson, J., Boyd, I., Kotkamp, M., Gomez, R. M., Murphy, M., Tran, H., and McGaw, J.: Evolution of observed ozone, trace gases, and meteorological variables over Arrival Heights, Antarctica (77.8° S, 166.7° E) during the 2019 Antarctic stratospheric sudden warming, Tellus B, 73, 1–18, https://doi.org/10.1080/16000889.2021.1933783, 2021.

Sofieva, V. F., Kalakoski, N., Verronen, P. T., Päivärinta, S.-M., Kyrölä, E., Backman, L., and Tamminen, J.: Polar-night O_3, NO_2 and NO_3 distributions during sudden stratospheric warmings in 2003–2008 as seen by GOMOS/Envisat, Atmos. Chem. Phys., 12, 1051–1066, https://doi.org/10.5194/acp-12-1051-2012, 2012.

Solomon, S.: Nitrogen chemistry in Antarctica: A brief review. Dynamics, Transport and Photochemistry in the Middle Atmosphere of the Southern Hemisphere, NATO ASI Series book series (ASIC), volume 321, 191–201, https://doi.org/10.1007/978-94-009-0693-8, 1990.

Solomon, S.: Stratospheric ozone depletion: a review of concepts and history, Rev. Geophys., 37, 275–316, https://doi.org/10.1029/1999RG900008, 1999.

Solomon, S. and Garcia, R. R.: On the distribution of nitrogen dioxide in the high-latitude stratosphere, J. Geophys. Res., 88, 5229–5239, https://doi.org/10.1029/JC088iC09p05229,1983.

Solomon, S. and Keys, J. G.: Seasonal variations in Antarctic NO_x chemistry, J. Geophys. Res., 97, 7971–7978, https://doi.org/10.1029/91JD01707, 1992.

Solomon, S., Smith, J. P., Sanders, R. W., Perliski, L., Miller, H. L., Mount, G. H., Keys, J. G., and Schmeltekopf, A. L.: Visible and near-ultraviolet spectroscopy at McMurdo Station, Antarctica: 8. Observations of nighttime NO_2 and NO_3 from April to October 1991, J. Geophys. Res., 98, 993–1000, https://doi.org/10.1029/92JD02390, 1993.

Stone, K. A., Solomon, S., Kinnison, D. E., and Mills, M. J.: On recent large Antarctic ozone holes and ozone recovery metrics, Geophys. Res. Lett., 48, e2021GL095232, https://doi.org/10.1029/2021GL095232, 2021.

Strahan, S. E., Douglass, A. R., Newman, P. A., and Steenrod, S. D.: Inorganic chlorine variability in the Antarctic vortex and implications for ozone recovery, J. Geophys. Res.-Atmos., 119, 14098–14109, https://doi.org/10.1002/2014JD022295, 2014.

Strahan, S. E., Douglass, A. R., and Damon, M. R.: Why do Antarctic ozone recovery trends vary?, J. Geophys. Res.-Atmos., 124, 8837–8850, https://doi.org/10.1029/2019JD030996, 2019.

Strode, S. A., Taha, G., Oman, L. D., Damadeo, R., Flittner, D., Schoeberl, M., Sioris, C. E., and Stauffer, R.: SAGE III/ISS ozone and NO_2 validation using diurnal scaling factors, Atmos. Meas. Tech., 15, 6145–6161, https://doi.org/10.5194/amt-15-6145-2022, 2022.

Struthers, H., Kreher, K., Austin, J., Schofield, R., Bodeker, G., Johnston, P., Shiona, H., and Thomas, A.: Past and future simulations of NO_2 from a coupled chemistry-climate model in comparison with observations, Atmos. Chem. Phys., 4, 2227–2239, https://doi.org/10.5194/acp-4-2227-2004, 2004.

Tabazadeh, A., Santee, M. L., Danilin, M. Y., Pumphrey, H. C., Newman, P. A., Hamill, P. J., and Mergenthaler, J. L.: Quantifying Denitrification and Its Effect on Ozone Recovery, Science, 288, 1407–1411, https://doi.org/10.1126/science.288.5470.1407, 2000.

Toon, G. C., Farmer, C. B., Lowes, L. L., Schaper, P. W., Blavier, J.-F., and Norton, R. H.: Infrared aircraft measurements of stratospheric composition over Antarctica during September 1987, J. Geophys. Res., 94, 16571–16596, https://doi.org/10.1029/JD094iD14p16571, 1989.

Valks, P., Pinardi, G., Richter, A., Lambert, J.-C., Hao, N., Loyola, D., Van Roozendael, M., and Emmadi, S.: Operational total and tropospheric NO_2 column retrieval for GOME-2, Atmos. Meas. Tech., 4, 1491–1514, https://doi.org/10.5194/amt-4-1491-2011, 2011.

van der A, R. J., Allaart, M. A. F., and Eskes, H. J.: Multi sensor reanalysis of total ozone, Atmos. Chem. Phys., 10, 11277–11294, https://doi.org/10.5194/acp-10-11277-2010, 2010.

van der A, R. J., Allaart, M. A. F., and Eskes, H. J.: Extended and refined multi sensor reanalysis of total ozone for

the period 1970–2012, Atmos. Meas. Tech., 8, 3021–3035, https://doi.org/10.5194/amt-8-3021-2015, 2015a.

Van der A, R. J., Allaart, M. A. F., and Eskes, H. J.: Multi-Sensor Reanalysis (MSR) of total ozone, version 2, Royal Netherlands Meteorological Institute (KNMI) [data set], https://doi.org/10.21944/temis-ozone-msr2, 2015b.

van Geffen, J., Van Weele, M., Allaart, M., and Van der A, R.: TEMIS UV index and UV dose operational data products, version 2, Royal Netherlands Meteorological Institute (KNMI) [data set], https://doi.org/10.21944/temis-uv-oper-v2, 2017.

van Geffen, J., Boersma, K. F., Eskes, H., Sneep, M., ter Linden, M., Zara, M., and Veefkind, J. P.: S5P TROPOMI NO_2 slant column retrieval: method, stability, uncertainties and comparisons with OMI, Atmos. Meas. Tech., 13, 1315–1335, https://doi.org/10.5194/amt-13-1315-2020, 2020.

van Geffen, J., Eskes, H., Compernolle, S., Pinardi, G., Verhoelst, T., Lambert, J.-C., Sneep, M., ter Linden, M., Ludewig, A., Boersma, K. F., and Veefkind, J. P.: Sentinel-5P TROPOMI NO_2 retrieval: impact of version v2.2 improvements and comparisons with OMI and ground-based data, Atmos. Meas. Tech., 15, 2037–2060, https://doi.org/10.5194/amt-15-2037-2022, 2022a.

van Geffen, J. H. G. M., Eskes, H. J., Boersma, K. F., and Veefkind, J. P.: TROPOMI ATBD of the total and tropospheric NO_2 data products, Report S5P-KNMI-L2-0005-RP, version 2.4.0, 202207-11, KNMI, De Bilt, the Netherlands [data set], https://doi.org/10.5270/S5P-9bnp8q8, 2022b.

Veefkind, J. P., Aben, I., McMullan, K., Förster, H., de Vries, J., Otter, G., Claas, J., Eskes, H. J., de Haan, J. F., Kleipool, Q., van Weele, M., Hasekamp, O., Hoogeveen, R., Landgraf, J., Snel, R., Tol, P., Ingmann, P., Voors, R., Kruizinga, B., Vink, R., Visser, H., and Levelt, P. F.: TROPOMI on the ESA Sentinel-5 Precursor: A GMES mission for global observations of the atmospheric composition for climate, air quality and ozone layer applications, Remote Sens. Environ., 120, 70–83, https://doi.org/10.1016/j.rse.2011.09.027, 2012.

Verhoelst, T., Compernolle, S., Pinardi, G., Lambert, J.-C., Eskes, H. J., Eichmann, K.-U., Fjæraa, A. M., Granville, J., Niemeijer, S., Cede, A., Tiefengraber, M., Hendrick, F., Pazmiño, A., Bais, A., Bazureau, A., Boersma, K. F., Bognar, K., Dehn, A., Donner, S., Elokhov, A., Gebetsberger, M., Goutail, F., Grutter de la Mora, M., Gruzdev, A., Gratsea, M., Hansen, G. H., Irie, H., Jepsen, N., Kanaya, Y., Karagkiozidis, D., Kivi, R., Kreher, K., Levelt, P. F., Liu, C., Müller, M., Navarro Comas, M., Piters, A. J. M., Pommereau, J.-P., Portafaix, T., Prados-Roman, C., Puentedura, O., Querel, R., Remmers, J., Richter, A., Rimmer, J., Rivera Cárdenas, C., Saavedra de Miguel, L., Sinyakov, V. P., Stremme, W., Strong, K., Van Roozendael, M., Veefkind, J. P., Wagner, T., Wittrock, F., Yela González, M., and Zehner, C.: Ground-based validation of the Copernicus Sentinel-5P TROPOMI NO_2 measurements with the NDACC ZSL-DOAS, MAX-DOAS and Pandonia global networks, Atmos. Meas. Tech., 14, 481–510, https://doi.org/10.5194/amt-14-481-2021, 2021.

Von Clarmann, T.: Chlorine in the stratosphere, Atmósfera, 26, 415–458, https://doi.org/10.1016/S0187-6236(13)71086-5, 2013.

von Savigny, C., Rozanov, A., Bovensmann, H., Eichmann, K.-U., Noel, S., Rozanov, V. V., Sinnhuber, B.-M., Weber, M., Burrows, J. P., and Kaiser, J.: The ozone hole break-up in September 2002 as seen by SCIAMACHY on ENVISAT, J. Atmos. Sci., 62, 721–734, https://doi.org/10.1175/JAS-3328.1, 2005.

Wargan, K., Weir, B., Manney, G. L., Cohn, S. E., and Livesey, N. J.: The anomalous 2019 Antarctic ozone hole in the GEOS Constituent Data Assimilation System with MLS observations, J. Geophys. Res.-Atmos., 125, e2020JD033335, https://doi.org/10.1029/2020JD033335, 2020.

Waugh, D. W. and Plumb, R. A.: Contour advection with surgery: A technique for investigating finescale structure in tracer transport, J. Atmos. Sci., 51, 530–540, https://doi.org/10.1175/1520-0469(1994)051<0530:CAWSAT>2.0.CO;2, 1994.

Waugh, D. W. and Polvani, L. M.: Stratospheric polar vortices, in: The Stratosphere: Dynamics, Transport, and Chemistry, edited by: Polvani, L. M., Sobel, A. H., and Waugh, D. W., Wiley, ISBN 978-0-875-90479-5, 2010.

Weimer, M., Kinnison, D. E., Wilka, C., and Solomon, S.: Effects of denitrification on the distributions of trace gas abundances in the polar regions: a comparison of WACCM with observations, Atmos. Chem. Phys., 23, 6849–6861, https://doi.org/10.5194/acp-23-6849-2023, 2023.

Wenig, M., Kühl, S., Beirle, S., Bucsela, E., Jähne, B., Platt, U., Gleason, J., and Wagner, T.: Retrieval and analysis of stratospheric NO_2 from the Global Ozone Monitoring Experiment, J. Geophys. Res., 109, D04315, https://doi.org/10.1029/2003JD003652, 2004.

Wespes, C., Hurtmans, D., Clerbaux, C., Santee, M. L., Martin, R. V., and Coheur, P. F.: Global distributions of nitric acid from IASI/MetOP measurements, Atmos. Chem. Phys., 9, 7949–7962, https://doi.org/10.5194/acp-9-7949-2009, 2009.

Wespes, C., Ronsmans, G., Clarisse, L., Solomon, S., Hurtmans, D., Clerbaux, C., and Coheur, P.-F.: Polar stratospheric nitric acid depletion surveyed from a decadal dataset of IASI total columns, Atmos. Chem. Phys., 22, 10993–11007, https://doi.org/10.5194/acp-22-10993-2022, 2022.

Williams, J. E., Boersma, K. F., Le Sager, P., and Verstraeten, W. W.: The high-resolution version of TM5-MP for optimized satellite retrievals: description and validation, Geosci. Model Dev., 10, 721–750, https://doi.org/10.5194/gmd-10-721-2017, 2017.

World Meteorological Organization (WMO): Scientific Assessment of Ozone Depletion: 2022, GAW Report No. 278, 509 pp., WMO, Geneva, Switzerland, ISBN 978-9914-733-97-6, 2022.

Yela, M., Parrondo, C., Gil, M., Rodríguez, S., Araujo, J., Ochoa, H., Deferrari, G., and Díaz, S.: The September 2002 Antarctic vortex major warming as observed by visible spectroscopy and ozone soundings, Int. J. Remote Sens., 26, 3361–3376, https://doi.org/10.1080/01431160500076285, 2005.

Zempila, M.-M., van Geffen, J. H. G. M., Taylor, M., Fountoulakis, I., Koukouli, M.-E., van Weele, M., van der A, R. J., Bais, A., Meleti, C., and Balis, D.: TEMIS UV product validation using NILU-UV ground-based measurements in Thessaloniki, Greece, Atmos. Chem. Phys., 17, 7157–7174, https://doi.org/10.5194/acp-17-7157-2017, 2017.